Chapter 2
Gold Nanostructures for Cancer Imaging and Therapy

Yongping Gao and Yongsheng Li

Abstract Gold nanostructures can manipulate light at the nanoscale based on the optical phenomenon widely known as localized surface plasmon resonance (LSPR). Upon light excitation, specific gold nanostructures are supposed to preferentially absorb or scatter light in the near-infrared (NIR) region, which enable them applicable as imaging and therapeutic agents. Furthermore, facile surface functionalization via Au-S bonding makes gold nanostructures as universal substrates to attach functional molecules, drug cargo, and targeting ligands. Together with their easy synthesis and non-toxicity, gold nanostructures have emerged as a greatly promising platform in cancer diagnostics and treatment. This chapter summarizes the progress made in cancer imaging and therapy with gold nanostructures (1) as therapeutic components for photothermal therapy, photodynamic therapy, chemotherapy, and their combination; (2) as probes for various imaging techniques including dark-field, optical coherence tomography, two-photon luminescence, photoacoustic imaging, computed tomography, and surface-enhanced Raman scattering based imaging; and (3) as a theranostic platform for imaging-guided therapy.

Keywords Gold nanostructures • Nanoshell • Nanorod • Nanocage • Photothermal therapy • Contrast agents • Imaging-guided therapy

2.1 Introduction

Gold nanostructures have emerged as a promising new platform in biomedical diagnostics and targeted therapeutics due to their unprecedented capability to manipulate light at the nanoscale and to integrate into biological systems [1, 2]. Most of these applications based on gold nanostructures come from an optical phenomenon known as localized surface plasmon resonance (LSPR), which is determined and highly tunable by the size and shape of the nanoparticle [3]. It can be tuned to

Y. Gao • Y. Li (✉)
East China University of Science and Technology,
130 Meilong Road, Shanghai 200237, China
e-mail: ysli@ecust.edu.cn

Z. Dai (ed.), *Advances in Nanotheranostics I*, Springer Series in Biomaterials Science and Engineering 6, DOI 10.1007/978-3-662-48544-6_2

preferentially absorb or scatter light at specific wavelengths in the visible and near-infrared (NIR) regions of the spectrum. In the NIR "tissue window," light penetration into tissue is optimal. Compared with conventional chemotherapy drugs or small-molecule imaging agents, gold nanostructures offer several advantages for biomedical applications, including high biocompatibility and noncytotoxicity [4], passive accumulation at tumor sites due to the enhanced permeability and retention (EPR) effect [5], and ease of bioconjugation via Au-S bonding to provide increased stability and active tumor targeting [6, 7].

Following excitation of LSPR by NIR laser, gold nanostructures tuned to absorb NIR irradiation are particularly useful as mediators for photothermal cancer therapy [8], to enhance contrasting effects in photoacoustic tomography [9] or to trigger thermosensitive release in drug-delivery systems [10–13]. Furthermore, the NIR light scattering of gold nanostructures has been applied for biomedical imaging such as dark-field microscopy and optical coherence tomography [14]. Other imaging modalities have also been integrated into gold nanostructures for imaging-guided therapy [15]. Over the past two decades, the pace of research in this field has advanced significantly and rapidly. It has been the present authors' best attempt to follow new developments in the field, but, given the pace of progress, this chapter will be partially outdated by the time it hits the press. This chapter is designed for researches already in the field to use it as a quick reference or "early-stage" researchers to gain a broader understanding of this field. The first section of this chapter will highlight the unique optical and material properties of gold nanostructures. Then, it will focus on the photothermal therapy based on various types of gold nanostructures. Also, the combination with other therapeutic approaches such as chemotherapy will be discussed. In the third section, gold nanostructures for diagnostics will be comprehensively described. Finally, gold nanostructures developed for imaging-guided therapy of cancer will be discussed.

2.2 Plasmonic Properties and Surface Functionalization of Gold Nanostructures

2.2.1 Radiative Properties

When light interacts with gold nanostructures, conduction electrons can be driven by the incident electric field in collective oscillations known as localized surface plasmon resonance (LSPR) [16]. Figure 2.1 illustrates this phenomenon for a gold nanosphere – the simplest type of LSPR (dipolar LSPR). This gives rise to a drastic alteration of electromagnetic fields on the gold surface with local field intensities which can be orders of magnitude greater than those of the incident field. The enhanced electromagnetic fields affect both radiative and nonradiative properties of gold nanostructures, resulting in absorption and light scattering following light incidence (Fig. 2.2). By adjusting the size and shape of gold nanostructures, the relative absorption and scattering behaviors can be controlled [3]. Small nanoparticles

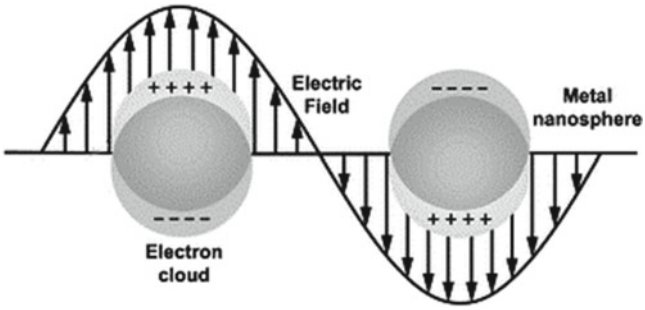

Fig. 2.1 Schematic illustration of LSPR of an individual gold nanosphere showing the collective oscillation of delocalized electrons in response to an external electric field

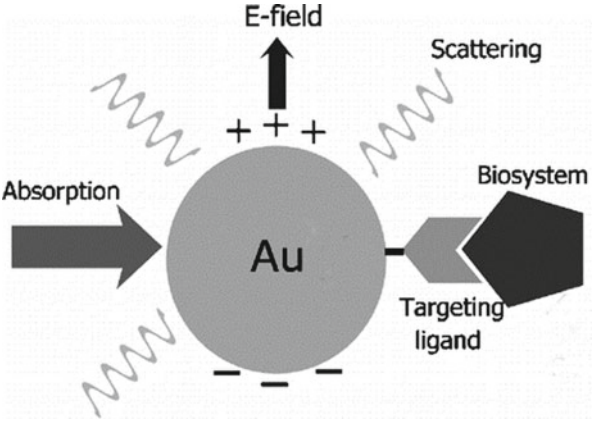

Fig. 2.2 Optical processes (radiative or nonradiative) resulting from the interaction of light with a gold nanoparticle

predominantly absorb light, while larger nanoparticles are largely scattering incident light. But for gold nanostructures with complex geometry, e.g., nanorods and nanostars, the absorption and scattering properties are dependent on their unique geometry greatly and their size on a small way [17]. Highly scattering gold nanostructures are particularly utilized as contrast agents for dark-field imaging [18, 19] and for computed tomographic (CT) imaging [20]. Moreover, the greatly intensified local field of gold nanostructures enhances the Raman signal of molecules in the vicinity of gold surface, enabling surface-enhanced Raman scattering (SERS)-based imaging [21].

Besides, by engineering the size, shape, and morphology of the nanostructure and the interparticle distance and dielectric environment, their LSPRs can be tuned from visible to the NIR region (700–1,400 nm) [22–24]. The NIR region is the so-called biological window defined as the spectral ranges where tissues become partially transparent due to the simultaneous reduction in both absorption and scattering [25, 26]. This is of particular interest for deep-tissue imaging and treatment.

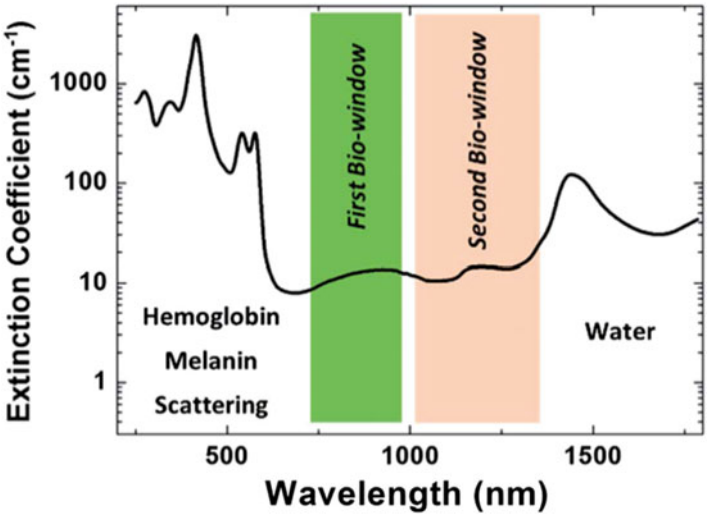

Fig. 2.3 Extinction coefficient of a representative tissue. The different effects leading to light attenuation (such as the presence of hemoglobin, water, and optical scattering) and the spectral extensions of the two biological windows are indicated (Reproduced from Ref. [17] by permission of The Royal Society of Chemistry)

Figure 2.3 shows the extinction spectrum of a typical human tissue [17]. The presence of several absorption bands is used to define two main biological windows. The first biological window extends from 700 to 980 nm, which was firstly proposed in 2001 [25] and has been extensively applied since then. In this spectral region, light absorption strongly vanishes but residual scattering still exists. The second biological window ranges from 1,000 to 1,400 nm, where optical absorption does not vanish completely; on the other hand, optical scattering is minimized. A range of gold nanostructures with variable shapes and sizes are shown in Fig. 2.4, and their tunable optical resonances are shown in Fig. 2.5. Since size-dependent LSPR tenability of gold nanospheres is quite limited (only in the visible region), the effective ways to achieve NIR plasmon resonance is usually by using nanoshells and anisotropic nanostructures. As seen from Fig. 2.5a, the plasmon peak shifts to the NIR region as branch aspect ratio of gold nanostars increases [27]. The long-axis LSPR peak redshifts from the visible to the NIR as the nanorod aspect ratio increases (Fig. 2.5b) [28]. Au nanocages (Fig. 2.5c) and nanoshells (Fig. 2.5d) show similar visible-NIR tunability of LSPR by facile control of the wall thickness and void size [29] and of the shell thickness (or thickness-to-core radius ratio) of the nanoshell [30], respectively.

Additionally, interparticle plasmonic coupling occurs when nanoparticles are brought in close proximity to one another as dimers, trimmers, and other higher-order clusters, leading to redshifts in LSPR and enhanced local electric field.

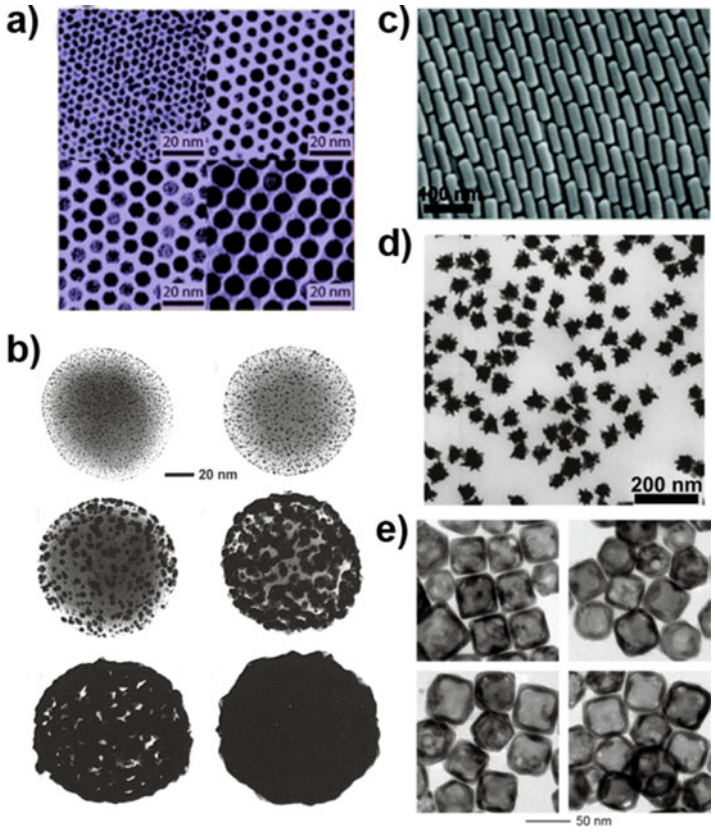

Fig. 2.4 TEM and SEM micrographs of gold nanostructures with various shapes and sizes: (**a**) nanospheres, (**b**) nanoshells, (**c**) nanorods, (**d**) nanostars, and (**e**) nanocages ((**a**) Reprinted with the permission from Ref. [31]. Copyright 2003 American Chemical Society. (**b**) Reprinted from Ref. [30], Copyright 1998, with permission from Elsevier. (**c**) Reprinted with the permission from Ref. [32]. Copyright 2012 American Chemical Society. (**d**) Reproduced from Ref. [33] by permission of IOP Publishing. (**e**) Reprinted with the permission from Ref. [34]. Copyright 2007 American Chemical Society)

Generally, the coupling does not occur until the interparticle separation is less than 2.5 times the particle diameter [35]. El-Sayed et al. proposed a universal relationship between the exponential decay of the spectral shift with respect to the interparticle separation [36]. Formation of gold nanostructure assemblies is not only distinguishable by clear redshift in the plasmon resonance but also by a dramatic change in solution color. These spectral and colorimetric changes have been harnessed in LSPR sensing of DNA, proteins, and biomolecules [37–40]. On the other hand, the significantly intensified local electric fields, also known as "hot spots" within the junctions of closely clusters, give rise to substantial enhancement in SERS enabling the detection of cancer cells [41–43].

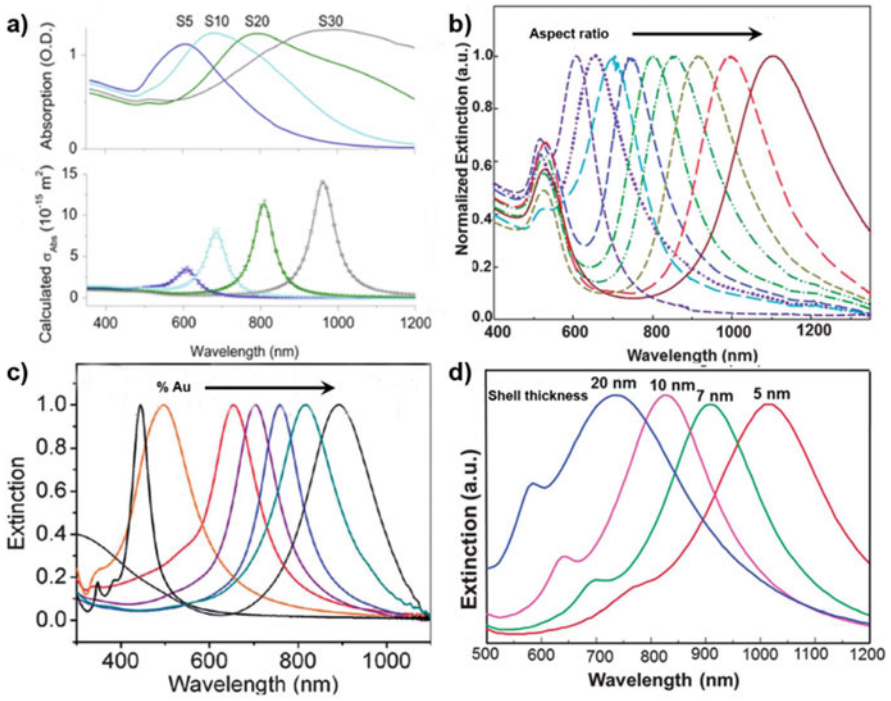

Fig. 2.5 Tunability of plasmon resonances achieved by varying the geometry of (**a**) nanostars, (**b**) nanorods, (**c**) nanocages, and (**d**) nanoshells [30] ((**a**) Reproduced from Ref. [27] by permission of IOP Publishing. (**b**) Reproduced from Ref. [28] by permission of IOP Publishing. (**c**) Reprinted by permission from Macmillan Publishers Ltd: Ref. [29], copyright 2007. (**d**) Reprinted from Ref. [30], Copyright 1998, with permission from Elsevier

2.2.2 Nonradiative Photothermal Effects

In addition to radiative decay, plasmons also relax nonradiatively through electron-electron collision or electron-lattice which generates light absorption by the nanoparticle [44]. Light to heat conversion has been extensively employed for photothermal therapy [45–48] and photothermal drug release in cancer cells [13, 49–52], as well as for two-photon luminescence imaging [27, 53]. The underlying mechanism of photothermal process has been extensively studied with ultrafast laser spectroscopy [22, 54]. Figure 2.6 illustrates the photothermal characteristics of gold nanostructures [15]. Upon excitation with the resonant photons, the photoexcitation of the electron gas results in rapid nonequilibrium heating. The initial electronic excitation is followed by relaxation at subpicosecond timescale (~30 ps) by means of electron-electron scattering which results in the surface temperature increase of the metal [55, 56], leading to the ablation of the nanoparticle, desorption of surface capping, or melting and reshaping. Then, cooling to equilibrium by energy exchange happens between the electrons and the lattice phonons. At slower

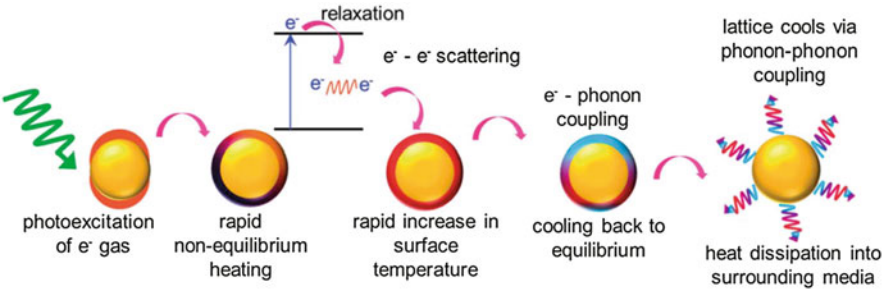

Fig. 2.6 Schematic illustration describing the principle of incident light to heat conversion by gold nanostructures (Reproduced from Ref. [15] by permission of The Royal Society of Chemistry)

rates, the lattice cools via phonon-phonon process (~100 ps) leading to heating of the local environment (surrounding medium). Thus, when gold nanostructures after incubation with cancer cells are illuminated, a large temperature difference between the hot nanoparticle surface and the much cooler surrounding biological medium occurs, resulting in an abrupt local temperature increment and the corresponding cell death.

The nonradiative properties of gold nanostructures also manifest themselves in the form of two-photon photoluminescence (TPL) of gold. An electron in the sp-conduction band is excited by the first photon from below the Fermi energy to above it via an intraband transition. This gives rise to a charge-separate state within the conduction band. An electronic transition from the *d*-band to *sp*-band occurs with a second-photon excitation, generating an electron-hole pair followed by recombination of separated charges resulting in TPL emission [57]. TPL based on variable gold nanostructures has been considerably investigated and applied for cancer imaging [58–62].

2.2.3 Surface Functionalization

The surface chemistry of gold is closely related to a number of critical attributes that make gold nanostructures a promising platform for biomedical applications. The nonreactive and relatively bio-inert nature of gold makes this metal a good candidate for both in vitro and in vivo applications. The low cytotoxicity of gold nanostructures, along with favorable clinical biocompatibility, has been demonstrated in a number of studies [63, 64]. Nevertheless, the synthetic reagent CTAB, for example, which is so crucial in a number of preparations of gold nanorods and other shapes, is highly toxic to cells at micromolar concentrations on its own [7]. The binding of toxic CTAB to a nanoparticle surface makes it far less bioavailable than it would be if it were free in solution. Thus, chemical tuning of the nanoparticle surface is still necessary to impart biological compatibility and specificity to gold nanoparticles.

Functional binding onto the surface of gold nanostructures for biomedical applications follows largely on work of self-assembled monolayers (SAMs), where molecules generate highly ordered monolayers once they adsorb onto a gold surface [65]. A rich variety of functional molecular linkers are currently employed in the conjugation of gold nanoparticles, and the anchoring groups utilized for attachment of these molecules to the gold surface generally include thiolate [66–68], dithiolate [69], dithiocarbamate [70], amine [71], carboxylate [71], selenide [72], isothiocyanate [68, 71], or phosphine [67, 73] moieties. Among these groups, thiolate and dithiolate are most well known for forming strong, stable gold-thiolate bonds (Au-S, ~50 kcal/mol) to molecules with thiol (-SH) or disulfide groups (S-S) [65]. By carefully choosing the functional groups at the distal end of the molecule, it is possible to design and generate a well-defined interface for better stability and interaction with cells and biomolecules in specific ways (Fig. 2.7). Apart from that, gold nanostructures can also adsorb biological molecules in a nonspecific manner. A variety of proteins will adsorb to a non-protected gold surface when it is transferred into a biological medium. The adsorbed proteins can affect the surface properties of gold nanostructures and thus their cellular uptake [7].

Thiolated poly(ethylene glycol), PEG-SH, is by far the most commonly employed surface ligand for gold nanostructures. It is a biocompatible polymer that helps prevent particle aggregation, nonspecific protein adsorption, and the uptake of circulating gold nanoparticles by the reticuloendothelial system (RES), allowing for longer circulation of gold nanoparticles in the bloodstream and consequently their greater accumulation in tumors through the enhanced permeability and retention (EPR) effect [74]. When the surface ligands for nanoparticle synthesis bind less strongly than gold thiolate interactions, their replacement with a thiol-terminated PEG is relatively straightforward [75].

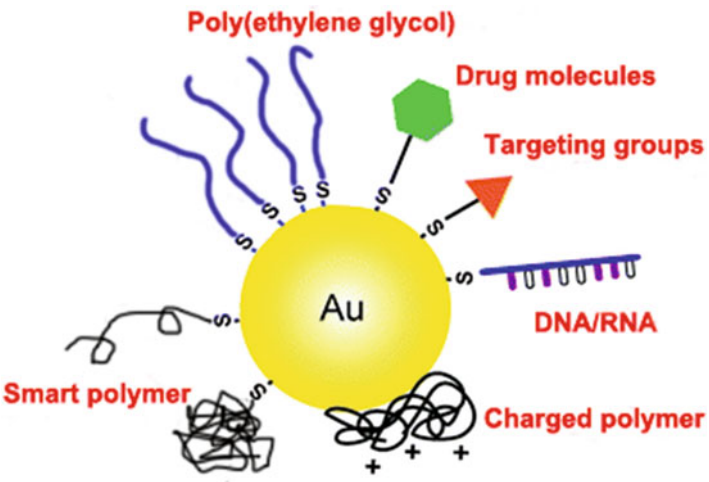

Fig. 2.7 Gold nanostructures can be conjugated with a wide variety of functional moieties

Gold nanostructures can be endowed with active targeting capabilities via careful surface modification. If nanoparticles are conjugated with a complimentary moiety (e.g., antibodies, peptides, and folate, among others), they will bind to cancer cells as they circulate, increasing their concentration in the desired region. Furthermore, the binding of the targeting moiety can either occur directly to the surface of the nanoparticle or to the terminal end of an attached PEG chain with an appropriate tail group [74, 75].

It is also possible to attach a number of other functional groups to the surface of gold nanostructures through thiolate binding, as shown in Fig. 2.7. For example, by adsorbing specific polymers to the surface, the charge of gold nanoparticle is supposed to be controlled, which is important as surface charges have a significant effect on both the cellular uptake and biodistribution of nanoparticles [76–78]. Inorganic complexes such as cisplatin or its prodrug forms can be bound to gold nanoparticle by way of appropriate ligands, which facilitate intracellular transport and subsequent activation of prodrug [79]. It is also simple to use the thiol group to attach for sensing applications, smart polymers for stealth delivery, as well as a wide variety of other types of molecules [13, 51, 71, 80–82].

Besides, gold nanoparticles could be fully encapsulated by silica (glass) shells by vitreophobic surface conjugation and facile silane chemistry [83–85]. This is of particular interest for use with gold nanorods, where CTAB molecules binding on the surface could be completely removed or displaced. Furthermore, Raman reporter molecules could be entrapped onto gold nanostructures followed by silica encapsulation, forming SERS probes with great potential in SERS detection [86].

2.3 Gold Nanostructures for Photothermal Therapy

Thermal treatments are based on driving a part of the body above its normal temperature for a defined period of time. Temperature plays an extremely important role in the dynamics and viability of biological system ranging from the simplest (cells) to the most sophisticated ones (tissues and organisms) [87]. In the case of human, any temperature increment above the normal body temperature (*circa* 37 °C) is usually regarded as a negative sign as it could indicate the presence of disease (fever) and even irreversible damage and fatal organ failure [88]. Nevertheless, controlled temperature increments could have positive effects in patients with an ongoing disease, such as cancer. In the last few years, great efforts have been put into the development of novel techniques for controlled and localized heating, along with understanding of the mechanisms on the basis of temperature-induced cell killing and modification [89, 90]. It is believed that the temperature-induced changes caused at the cellular level are unequivocally determined by the intensity and duration of the increment [91]. Depending on the magnitude of the induced temperature increment, thermal treatments and related effects on tumors would be classified into several periods, as depicted in Fig. 2.8 [92]. By increasing the tumor temperature above 48 °C during a period of time (a few minutes), irreversible injury treatments

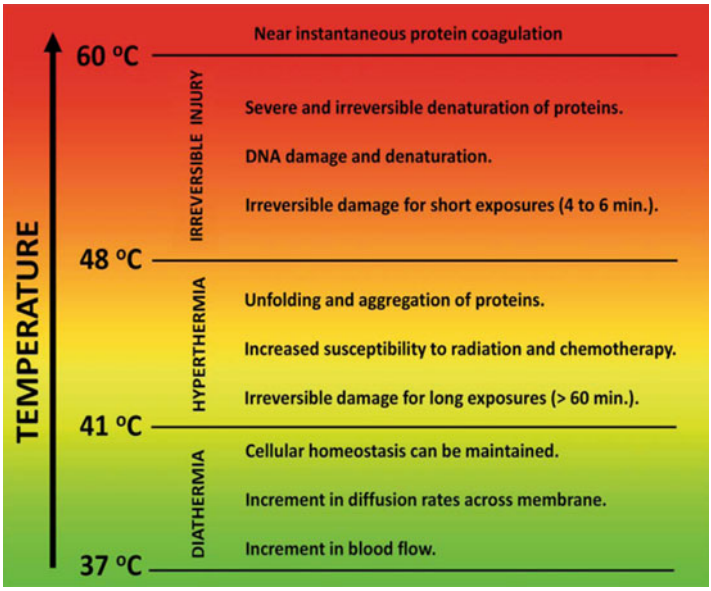

Fig. 2.8 Schematic diagram of the variety of effects caused by the different thermal treatment as classified by the corresponding operating temperature (Reproduced from Ref. [17] by permission of The Royal Society of Chemistry)

would occur. In this case, a drastic activation of cell death is achieved as a consequence of coagulative necrosis processes. As it is increased above 60 °C, an almost instantaneous and irreversible protein denaturation will be caused. These treatments are considered highly efficient but lack selectivity accompanied by relevant collateral damage to adjacent tissue. Within 41–48 °C temperature, tumor would experience hyperthermia treatments. Several processes of relevance at the cellular level are supposed to be simultaneously activated, including protein denaturation, transient thermo-tolerance, and cell inactivation. Temperature up to 41 °C does not induce relevant modifications at the cellular level, which is mainly applied in physiotherapy favoring muscle relaxation and pain relief.

Recently, the development of nanoparticles capable of efficient heat generation with laser irradiation has attracted much attention [93]. In particular, gold nanostructures with plasmonic properties tailored into NIR region have shown great promise for cancer photothermal therapy through nonradiative photothermal effect, demonstrating the ability to destroy cancerous lesion in vivo [94]. A diverse range of gold nanoparticles have been explored for use in phothermal therapy [95, 96]. Key features to consider when selecting a nanostructure for photothermal therapy are the plasmon resonance wavelength, the absorption cross section, and the size of the nanoparticle. In this section, the development of gold nanostructures including nanoshells, nanorods, nanocages, and other anisotropic gold nanoparticles for photothermal therapy will be discussed. Besides, as single photothermal therapy is not as effective as we expected, for example, caused by thermo-tolerance of cancer

cells [97], the combination of photothermal therapy with other therapeutic strategies, mainly photodynamic therapy and chemotherapy, has received tremendous interest in recent years [98–102], which will be covered in the second section.

2.3.1 Gold Nanoshells

Gold nanoshells are usually core/shell nanoparticles comprising a dielectric silica core surrounding by a gold shell and can be easily synthesized through the seed-mediated growth process [30, 103, 104]. As their LSPR can be easily tuned to NIR region by simply modifying the core-to-shell ratio, gold nanoshells were the first sample used to demonstrate photothermal cancer therapy, and now the transition of this approach to clinical trials is currently underway [105]. In 2003, Hirsch et al. [45] studied the temperature distribution in tumors during thermal therapy and highlighted the merits of injecting nanoshells directly into the tumor interstitium rather than administering them intravenously. The mean change in temperature for the nanoshell group (37.4 ± 6.6 °C) was high enough to cause irreversible thermal damage, whereas the more modest temperature increase in the nanoshell-free control group (9.1 ± 4.7 °C) was insufficient to cause any permanent damage. Interestingly, the heating profile was approximately homogeneous, which indicated that the tumor volume contained a near-uniform distribution of nanoshells. The maximum high temperature was measured approximately 1 mm below the surface and not at the site of injection. In another study in 2004, O'Neal et al. [106] have successfully treated mice inoculated with tumors after injection with PEGylated nanoshell solution via tail vein. A complete resorption of tumors was observed within 10 days, and all mice were healthy and free of tumors at 90 days. By contrast, in the control groups, the tumors continue to grow after treatment, with a mean survival time of 10.1 days.

Except for silica, different materials have been used as cores of nanoshells. Liu and coworkers reported a new approach toward the design of nanoshells on carboxylated polystyrene [107]. The tumor volumes of the treatment group by the nanoshells injected intraperitoneally were significantly lower than those of the control groups, with an average inhibition rate over 55 %. Recently, lipid vesicles, mesoporous silica, and other functional nanoparticles have also been used as the template to prepare nanoshells as photothermal therapy agents [108–111]. Furthermore, because of the ease of surface functionalization, gold naoshells are often conjugated with targeting ligands for targeted photothermal therapy [98]. In 2009, Li and coworkers investigated in vivo tumor targeting by PEGylated nanoshells conjugated with a melanocyte-stimulating hormone (MSH) analogue for selective photothermal ablation of melanoma tumors [112]. In the meantime, it is found that intravenous injection of RGD peptide-conjugated nanoshells could target glioma tumors for photothermal treatment which significantly prolonged the survival of tumor-bearing mice [113].

Gold nanoshells have a significantly larger photothermal transduction cross section, compared to gold nanorods on a per particle basis [114]. However, the lower

absorption efficiency of gold nanoshells, usually below 60 % (much lower than that of gold nanorods, above 90 %) [114, 115], greatly limits their applications in photothermal therapies. By encapsulating gold cores into gold nanoshells, a gold-silica-gold multilayered nanoshell structure, known as a simple "nanomatryoshka" [24], has been created to provide a higher plasmonic tunability. Theoretically, the relative absorption and scattering efficiencies can be tuned in a wider range by controlling the geometry [116]. In a recent work, Halas and coworkers [117] calculated that the absorption efficiency for a nanomatryoshka with plasmon resonance at about 800 nm is 4.26, which corresponds to 77 % of the total extinction efficiency of 5.53 (Fig. 2.9). These nanomatryoshkas show a scattering efficiency of 1.26, 23 % of their extinction efficiency. For nanoshells exhibiting the similar plasmon resonance, the major contribution to the total extinction comes from a scattering efficiency of 7.25, which represents 85 % of the extinction efficiency, with a minor contribution from the absorption efficiency of 1.24, only 15 % of the total extinction efficiency.

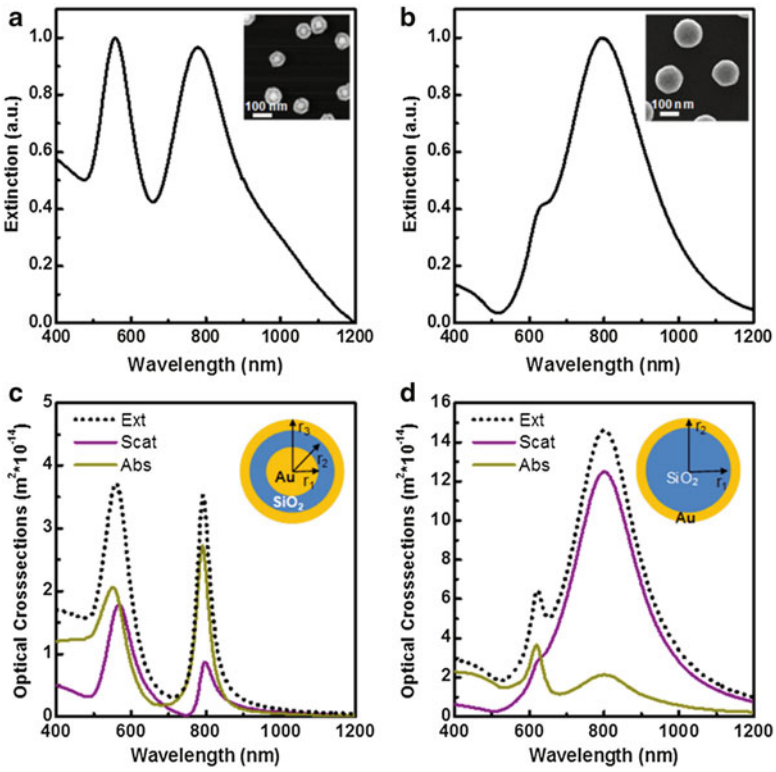

Fig. 2.9 Optical and structural properties of nanomatryoshka and nanoshells. Experimental ensemble extinction spectra of nanomatryoshkas (**a**) and nanoshells (**b**). Calculated extinction, scattering, and absorption cross-section spectra (Mie theory) of the $[r_1, r_2, r_3] = [21, 31, 44]$ nm nanomatryoshka (**c**) and the $[r_1, r_2] = [62, 76]$ nanoshell (**d**) (Reprinted with the permission from Ref. [117]. Copyright 2014 American Chemical Society)

The larger absorption efficiency and smaller scattering efficiency of nanomatryoshkas will result in higher photothermal transduction efficiency than that of the gold nanoshells. Furthermore, after an intravenous injection of Au nanomatryoshkas followed by a single NIR laser dose of 2 W/cm^2 for 5 min, 83 % of the TNBC tumor-bearing mice appeared healthy and tumor-free >60 days later, while only 33 % of mice treated with nanoshells survived the same period. The combination of smaller size and larger absorption cross section of Au nanomatryoshkas makes this nanoparticle more effective than gold nanoshells for photothermal cancer therapy. In another study, sub 100 nm gold nanomatryoshkas comprising concentric gold-silica-gold layers were demonstrated to accumulate into tumor with four- to fivefold the amount of gold nanoshells following equal dose of injected gold [118]. The survival time of mice-bearing large (>1,000 mm^3) and highly aggressive triple-negative breast tumors is doubled for the nanomatryoshka treatment group under identical photothermal therapy conditions. Li and coworkers [119] have successfully developed a facile but controllable approach for the fabrication of the simple nanomatryoshka, in which organosilica layer was chosen as the dielectric spacer layer. Upon near-infrared (NIR) laser irradiation, nanomatryoshka performed much better than conventional gold nanoshells at the same extinction intensity and could kill cancer cells efficiently both in vitro and in vivo.

More excitingly, it is reported that gold nanoshells, as an effective class of photothermal agents, have entered clinic trails. Recently, Cancer Treatment Centers of America (CTCA) and Nanospectra Biosciences have carried out the first clinical trial for the treatment of primary and/or metastatic lung tumor by Aurolase therapy that uses Auroshell (Fig. 2.10) based on gold nanoshells invented by Halas's group at Rice University. The therapy begins with an intravenous deliver of Auroshell, and

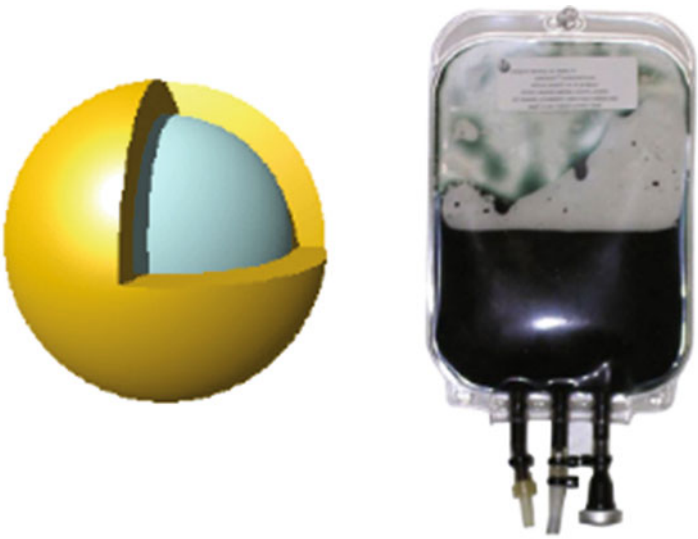

Fig. 2.10 Individual auroshell particle (*left*) and IV bag of auroshell (*right*)

after 12–24 h, for the tumor accumulation, a NIR laser is used to illuminate and destroy tumors in the patient. It is known that this clinical trial is in phase II stage right now [120].

2.3.2 Gold Nanorods

Gold nanorods, which were developed during the same period as gold nanoshells, are generally smaller than nanoshells. They have been extensively explored in photothermal therapy due to their strong optical extinction in the visible and NIR region [121]. By simple manipulation of the aspect ratio of nanorods, the strong longitudinal plasmon resonance band of gold nanorods can be tuned into NIR region. Recent studies have investigated the photothermal heating efficiencies of NIR-absorbing gold nanostructures, and both theoretical and experimental results have shown that nanorods could offer a superior absorption cross section versus gold nanoshells when normalizing for particle size differences as well as heating per gram of gold that is at least six times faster than gold nanoshells [114, 122, 123].

There have been numerous examples of gold nanorods used for in vivo photothermal cancer therapy. Van Maltzahn et al. reported that PEG-coated gold nanorods could be used as an efficient photothermal nanoheater [123]. In their work, PEGylated nanorods exhibited a long blood half-life of ~17 h after intravenous injection into tumor-bearing mice and could accumulate in tumor at ~7 % ID/g at 72 h postinjection. It was found that the tumors of the treatment group were rapidly heated to over 70 °C by laser irradiation (810 nm, 2 W/cm^2, 5 min), whereas the control mice showed the maximum surface temperature at ~40 °C (Fig. 2.11). Thus, tumors on mice that received PEGylated nanorods through intravenous injection completely disappeared within 10 days after NIR laser irradiation, in marked contrast to the control groups with uninhibited tumor growth. Moreover, the survival time of mice of treatment groups was over 50 days as compared to ~33 days for control groups. Similar results of PEGylated gold nanorods for photothermal cancer treatment have also been reported by Dickerson et al. [124].

Similar to gold nanoshells, active tumor targeting with gold-nanorod bioconjugates for effective in vivo photothermal therapy has also been achieved by a number of groups. Choi et al. loaded gold nanorods into chitosan-conjugated pluronic-based nanocarriers that could selectively target the tumor [125]. The nanorods showed a rather high tumor uptake at over 20 % ID/g as compared with ~7 % ID/g for PEG modified nanorods. After intravenous injection and the followed NIR laser irradiation, tumor thermolysis was achieved, without showing any apparent damage to the surrounding healthy tissues (Fig. 2.11). In another work, Li et al. demonstrated tumor targeting and photothermal treatment using dendrimer-modified gold nanorods conjugated with arginine-glycine-aspartic acid (RGD) peptide [126]. The biodistribution study revealed the gradually increased tumor uptake of RGD

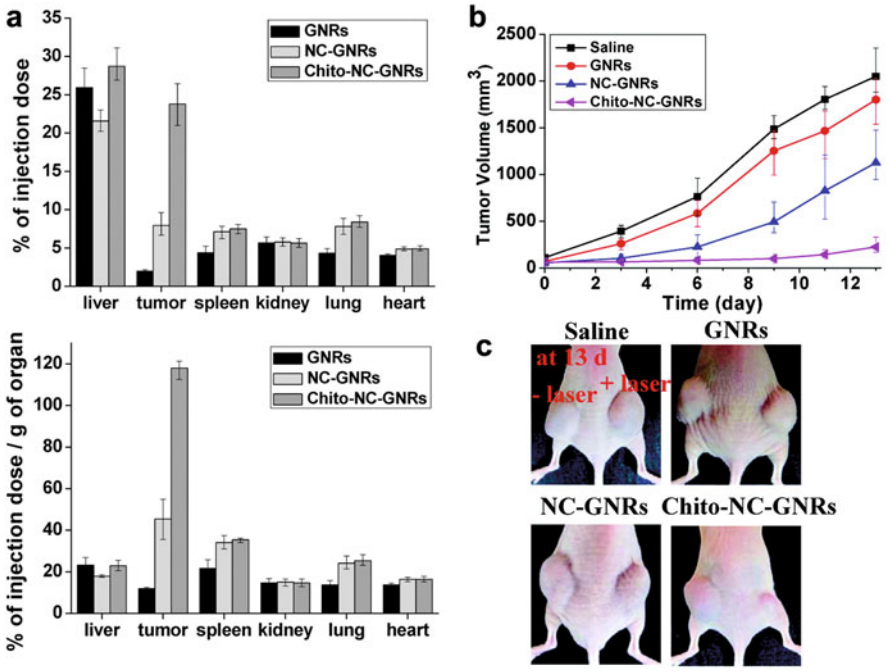

Fig. 2.11 (**a**) Biodistribution of GNRs or GNR-loaded nanocarriers in nude mice at 24 h after intravenous (tail vein) injection. (**b**) Changes in tumor volumes and (**c**) the tumor images after onetime NIR laser irradiation (808 nm, 4 W/cm^2) for 4 min at 24 h after the i.v. injection of the nanomaterials (Reprinted with the permission from Ref. [125]. Copyright 2011 American Chemical Society)

nanorods over time, and disappearance of tumors was observed after the intravenous injection and NIR laser irradiation.

On the other hand, a major challenge to the use of gold nanorods for photothermal therapy is their susceptibility to reshaping into gold nanospheres under intense laser illumination, resulting in a loss of the longitudinal NIR resonance. Horiguchi et al. reported that CTAB could enhance heat isolation and cause the nanorods to reshape [127]. Photothermal reshaping also strongly depends on the surface conditions of the particle [128, 129, 130]. Chon et al. implemented a simple heat-diffusion model to estimate the heat relaxation time of gold nanorods encased in silica shells [129, 130]. They found that heat dissipation in the silica shell was much faster than the gold-nanorod-reshaping process, resulting in the shell inhibiting nanorod reshaping. Thus, silica coating could render gold-nanorod higher photothermal stability, as well as the biocompatibility resulting from the elimination of CTAB by the coating of silica layer. This is anticipated to have wide biomedical applications in cancer therapy [11, 131].

2.3.3 Gold Nanocages

Gold nanocages represent another novel class of nanostructures firstly developed by Xia and coworkers [132–134]. Gold nanocages are created by hollowing out the interior of a sacrificial template of silver nanocubes (as well as silver nanocrystals with other shapes). When silver nanocubes are titrated with a gold salt (typically $HAuCl_4$), a galvanic replacement reaction occurs, causing gold atoms to be deposited on the surface of the nanocube and silver atoms to be dissolved from a small pit in the surface. By increasing gold replacement, the LSPR peak position of gold nanocages is tunable through the visible and into the NIR region.

In 2007, Xia's group demonstrated the selective photothermal destruction of SK-BR-3 breast cancer cells in vitro with gold nanocages functionalized by the anti-HER-2 antibody [47]. After incubation with the immune nanocages, SK-BR-3 breast cells were irradiated with a femtosecond laser at various power densities for 5 min. A well-defined area of cellular death corresponding to the laser spot was observed. Later in 2010, they examined the efficacy of gold nanocages for photothermal cancer treatment in mice (Fig. 2.12) [135]. After intravenous injection of PEGylated gold nanocages for 3 days, the tumor on each mouse was irradiated with an 808 nm continuous-wave laser at a power density of 0.7 W/cm^2 for 10 min. It is measured that the temperature of the tumors containing nanocages was rapidly heated to over 55 °C, leading to effective ablation of the tumors. In another study, they demonstrated that breast cancer stem calls (CSC) were targeted and eradicated through photothermal treatment with gold nanocages by functionalizing their surface with SV 119, a synthetic small molecule capable of binding to the sigma-2 receptor with high specificity [136].

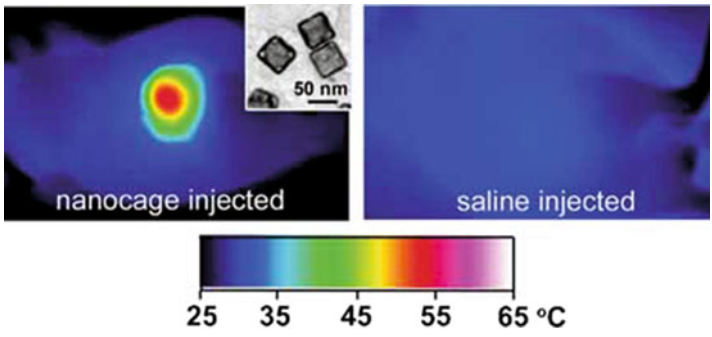

Fig. 2.12 IR thermal images of nanocage-injected (*left*) and saline-injected (*right*) tumor-bearing mice. The *inset* shows a TEM image of the as-made gold nanocages (Reproduced from Ref. [135] by permission of John Wiley & Sons Ltd)

2.3.4 Other Gold Nanostructures

Another type of gold nanostructures with NIR absorption for photothermal therapy is gold nanostars, which were spherical nanoparticles with multiple sharp edges and a high absorption-to-scattering ratio in the NIR region, favorable for photothermal heat generation [137, 138]. Lu et al. reported a multifunctional nanostars-based SERS assay for targeting sensing, photothermal treatment, and in situ monitoring of the photothermal response during the therapy process [138]. When nanostars were attached to cancerous cells, the localized heating that occurred during NIR irradiation was able to cause irreparable cellular damage. In another study, TAT-peptide functionalized nanostars were demonstrated to enter cells significantly more than bare or PEGylated gold nanostars [58]. After 4 h incubation of TAT-nanostars with BT549 breast cancer cells, efficient photothermolysis was accomplished using 850 nm pulsed laser under 0.2 W/cm^2 irradiation, which was among the lowest power densities ever reported for pulsed lasers and below the maximal permissible exposure of skin. The photothermal ablation in vivo was further demonstrated using PEGylated gold nanostars [59]. On a mouse injected systemically with PEGylated nanostars for 2 days, extravasation of nanostars was observed, and localized photothermal ablation was demonstrated on a dorsal window chamber with 10 min of irradiation (785 nm, 1.1 W/cm^2).

In addition, there are some other types of gold nanostructures with NIR absorption useful for photothermal therapy. Xia et al. synthesized gold hexapods and compared them with gold nanorods and nanocages [48]. They found that gold nanohexapods exhibited the highest cellular uptake and the lowest cytotoxicity in vitro for both the as-prepared and PEGylated samples. The PEGylated nanohexapods also showed significant blood circulation and tumor accumulation after intravenous injection. More importantly, the nanohexapods could significantly decrease the tumor metabolic activity following photothermal treatment after systemic administration. Another nanostructure, gold/gold sulfide NIR-absorbing nanoparticles (35–55 nm), was exploited to provide higher absorption (98 % absorption and 2 % scattering) as well as potentially better tumor penetration [139]. The ability to ablate tumor cells in vitro and efficacy for photothermal cancer therapy is demonstrated, and an in vivo model shows enhanced circulation and biodistribution and significantly increased long-term, tumor-free survival after photothermal treatment.

Though intensive effort has focused on shifting the absorbance of nanoparticles to the first biological window (650–900 nm) region for photoinduced therapy, gold nanostructures with plasmon absorption in the second biological window are also of great interest. Pelaz et al. described a novel and straightforward wet-chemical synthetic route to produce biocompatible single-crystalline gold nanoprisms [140], which could effectively ablate Vero cells after 2 min of 1,064 nm NIR illumination at 30 W/cm^2, which however was a rather high power density. Recently, Min-Fong Tsai et al. reported that a Au nanorod can be designed with a rod-in-shell (rattle-like) structure (Fig. 2.13a) smaller than 100 nm that is tailored to be responsive to

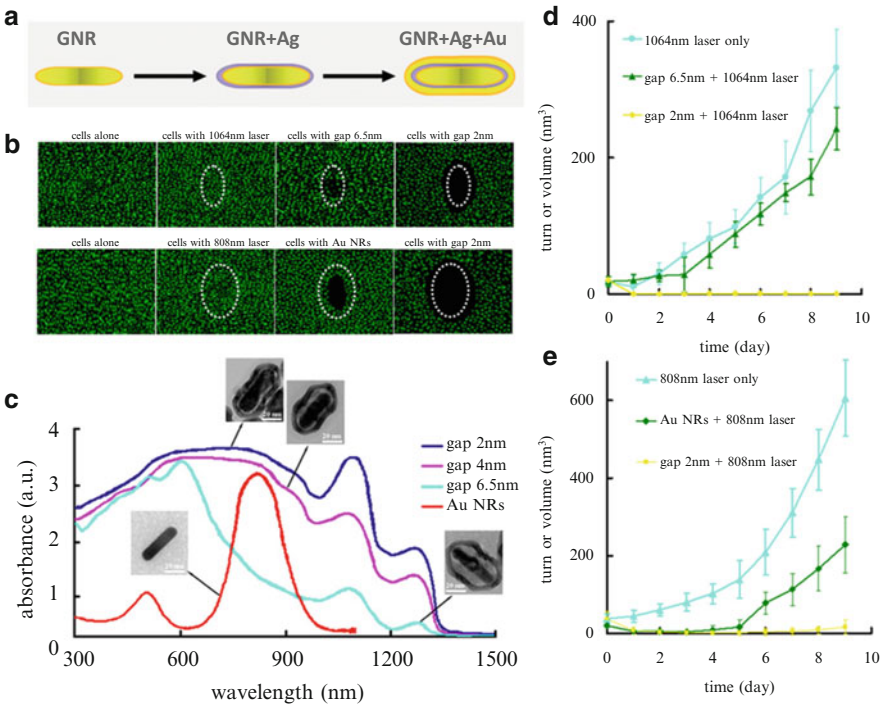

Fig. 2.13 (**a**) A schematic representation of the approach for the development of the rod-in-shell structure. (**b**) LLC/LL2 lung cancer cells treated with gap 6.5 nm and gap 2 nm rod in shells were irradiated using a 1,064 nm laser at 3 W/cm^2 for 5 min of exposure (*top*), and LLC/LL2 lung cancer cells treated with Au NRs and gap 2 nm rod-in-shells were irradiated using a diode 808 nm (*bottom*). The group of "cells with laser" was performed without treatment of rod in shell and exposed to laser. (**c**) The UV-vis-NIR spectra of Au rod in shells with different gaps and Au nanorods, and their corresponding TEM images. (**d**, **e**) Time-dependent tumor growth as a function of postirradiation days (Reprinted with the permission from Ref. [141]. Copyright 2013 American Chemical Society)

the first and second NIR windows [141]. In vitro performance clearly displays high efficacy in the NIR photothermal destruction of cancer cells, showing large cell-damaged area beyond the laser-irradiated area (Fig. 2.13b). Then, they tailored the plasmon resonances of the rod-in-shell structure by changing the gap distance between the nanorod core and the Au/Ag nanoshell, to evaluate the therapeutic effect of using a 1,064 nm diode laser (Fig. 2.13c). It was found that the mice injected with the 2 nm gap showed effective suppression of tumor growth under irradiation of 1,064 nm laser for 7 min (Fig. 2.13d). Furthermore, regarding the first NIR window with the use of an 808 nm laser, the photothermal ablation of solid tumors demonstrates that the rod in shell exhibits a more effective anticancer efficacy compared to Au nanorods (Fig. 2.13e).

2.4 Combination of Photothermal Therapy with Other Therapeutic Approaches

Numerous preclinical and clinical studies have proved that monotherapy (e.g., hyperthermia, chemotherapy, radiotherapy, surgery, and some other therapeutics) is not as effective as we expected [142, 143], due to incomplete tumor eradication, metastasis of cancer, development of drug resistance, individual differences in cancer patients, and so on [144–146]. Combination therapy, which uses more than one therapeutic approach, has shown great potential for the treatment of cancer and some other serious diseases [143, 147]. Combination of photothermal therapy with other therapeutic strategies based on gold nanostructures, such as photodynamic therapy and chemotherapy, has thus received tremendous interest in recent years.

2.4.1 Combination of Photothermal Therapy with Photodynamic Therapy

Photodynamic therapy generally falls into phototherapy, along with photothermal therapy. Both of them are deemed as minimal invasive and effective approaches for cancer treatment. Photodynamic therapy relies on the photosensitizer to transfer photo energy to the surrounding oxygen molecules, generating reactive oxygen species, such as singlet oxygen (SO), to kill tumor cells [148]. Owing to the tumor targeting ability of appropriately designed photosensitizers or photothermal agents based on gold nanostructures, as well as the selective light irradiation of the lesion region, combination of photothermal therapy and photodynamic therapy exhibits remarkably reduced side effects and improved selectivity compared with traditional remedies.

Jang and coworkers demonstrated that Al(III) phthalocyanine chloride tetrasulfonic acid (AlPcS4)-loaded gold nanorods could contribute to a strong reduced tumor growth effect (95 % inhibition) after combination of photothermal treatment and photodynamic treatment upon their intravenous injection, while the tumor growth inhibition effect was 79 % for those only receiving photodynamic therapy [149]. In another work by Wang and coworkers, an aptamer switch probe (ASP) linking chlorin e6 (Ce6), a photosensitizer molecule, to the surface of nanorods was constructed [150]. In the presence of target cancer cells, the ASP changes conformation to drive Ce6 away from the gold surface, thereby producing singlet oxygen for photodynamic upon light irradiation. Combined with destruction by the photothermal effect of gold nanorods, a remarkable and synergistic therapeutic effect compared to photothermal and photodynamic alone was observed for cancer cells.

In the abovementioned studies, two different lasers are independently used to trigger photothermal and photodynamic, separately. To simplify the treatment process, it would be helpful to find new strategies to accomplish photothermal and photodynamic treatment under a single laser irradiation. Chen et al. fabricated gold vesicles

composed of Ce6-loaded plasmonic vesicular assemblies of gold nanoparticles with strong NIR light absorbance in the NIR region of 650–850 nm [151]. Upon their intratumoral injection, effective combined photothermal and photodynamic treatment under a 671 nm laser irradiation was achieved. Furthermore, they constructed gold nanostars-PEG-Ce6 for coordinated photothermal/photodynamic therapy upon single CW laser irradiation both in vitro and in vivo [152]. It was demonstrated that the difference in photostability between photosensitizers and gold nanostructures could be used to modulate photothermal and photodynamic by adjusting irradiation time (Fig. 2.14), and the strategy significantly improved the anticancer effect and greatly simplified the treatment process. More recently, Kuo Chu Hwang and coworkers developed a unique morphology of a gold nanostructure, called nanoechinus (Fig. 2.15), [153] which sensitized the formation of singlet oxygen as well as exerted in vivo photodynamic and photothermal therapeutic effects in both the first and the second NIR biological windows for complete destruction of tumors in mice. The gold nanoechinus exhibits exceptionally high extinction coefficients at NIR biological window, seven to nine orders higher than conventional organic dyes and photosensitizers and three to four orders higher than that of gold nanoparticles, which are especially useful in deep-tissue-buried tumor treatment with a much lower amount of nanomaterials or lower incident light intensities/irradiation time.

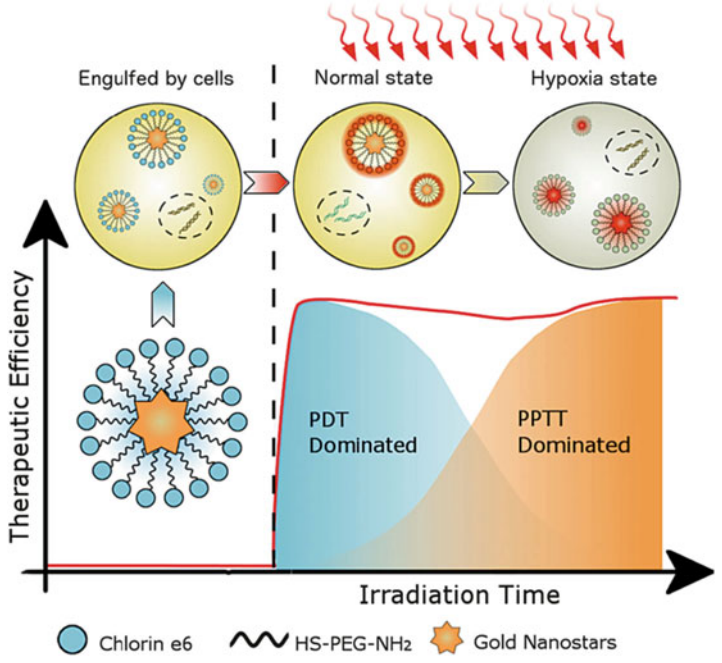

Fig. 2.14 Schematic illustration for explaining coordinated photothermal and photodynamic treatment upon single laser irradiation (Reproduced from Ref. [152] by permission of John Wiley & Sons Ltd)

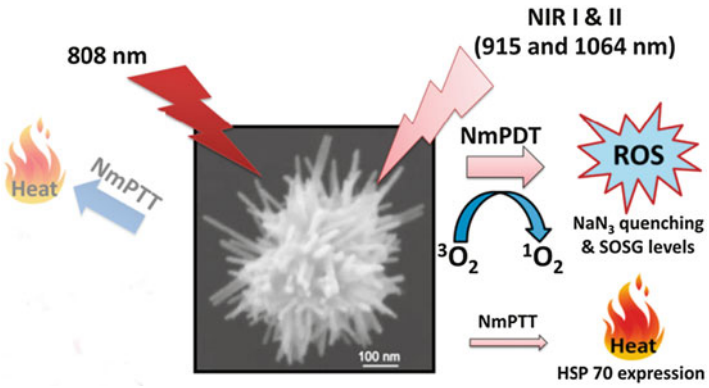

Fig. 2.15 Schematic representation of the working mechanisms of NIR light-induced photothera-peutic effects exerted by gold nanoechinus (Reproduced from Ref. [153] by permission of John Wiley & Sons Ltd)

The LSPR of gold nanostructures could be fine-tuned to overlap with the absorption of photodynamic dye with poor photostability and low quantum yield. Such overlap greatly increases the singlet oxygen yield by maximizing the local field enhancement and protecting photodynamic dye against photodegradation, thus enhancing the efficacy of photodynamic therapy. Very recently, Li et al. designed and validated a novel plasmon-enhanced photodynamic therapy for breast tumor by fabricating a nanoplatform composed of mesoporous silica-coated gold nanorods incorporating indocyanine green (ICG) [154]. The LSPR peak of the nanorod core has been regulated to overlap with the excitation band of ICG, thus increasing the absorption coefficient of incorporated ICG by virtue of the local enhanced field effect. The Au NR@SiO_2-ICG formulation dramatically increases the singlet oxygen generation under laser excitation, relative to free ICG, and demonstrates enhanced photodynamic destruction of human breast carcinoma MDA-MB-231. With mild laser irradiation, the growth of orthotopic breast tumors in mice was greatly inhibited through a synergistic effect of photodynamic and photothermal treatment.

2.4.2 Combination of Photothermal Therapy with Chemotherapy

Chemotherapy, one of the most commonly used cancer treatments, often causes systemic side effects due to unspecific drug delivery to all tissues including healthy ones. As a result, overall treatment efficacy is lowered by dose-limiting drug toxicity, and safe dosages may not completely eradicate tumors. In addition, half of all

chemotherapy patients develop drug resistance, a situation that also leads to treatment failure [155]. Temperature rise, induced by photothermal therapy, is sufficient to increase vascular permeability within tumors that have inefficient blood flow through their newly formed immature blood vessels, leading to selective drug delivery and enhanced cytotoxicity [156]. The combination of photothermal therapy and chemotherapy has proved to be effective on optimizing the efficacy of cancer treatment [157]. In recent years, various gold nanostructures with suitable surface modification have been extensively explored for the combined photothermal therapy and chemotherapy [100].

Gold nanoparticles have found various applications in the field of nanomedicine, which can be easily prepared in a size-controllable manner [95, 158]. You and coworkers prepared drug-delivery vehicles that encapsulate doxorubicin (DOX) with a pH-sensitive matrix embedded with gold nanoparticles. Such a nanostructure exhibited a high absorption in the NIR region. After being conjugated with a targeting moiety (Herceptin), the obtained drug carrier could be selectively engulfed by cancer cells, resulting in a combined therapeutic effect under the NIR laser irradiation [159]. In another study, Nam et al. designed a pH-responsive gold nanoparticle-based drug carrier, which could form aggregates in tumor regions by responding to micro acidic environment of the tumors [160]. Highly spatiotemporally concerted drug release and dramatically increased NIR light absorption were then observed, contributing to an effective synergistic tumor suppression effect in mouse xenografts.

Gold nanoshells prepared via various methods with strong NIR light absorptions are a useful nanoplatform for photothermal combination therapy. In 2010, Lee and coworkers fabricated an interesting half-nanoshell on the template of DOX-loaded PEG-PLGA nanomicelle, with plasmon absorption at 790 nm [161]. Under NIR laser irradiation upon intravenous injection, the intratumoral temperature was increased to 50–70 °C and DOX was rapidly released. Such a combination could result in the complete destruction of tumors without weight loss or tumor recurrence. Neither chemotherapy with a slightly higher dose of DOX nor the photothermal therapy alone without DOX could achieve the similar result. Recently, gold nanoshells consisting of a mesoporous silica nanorattle core and a thin outer gold nanoshell (SN@AuNSs) have been designed and synthesized by Tang et al. [108]. The amount of docetaxel (DOC) loaded in SN@AuNSs could reach up to 52 %. Both in vitro and in vivo results showed that the synergistic efficacy was much better than that of chemotherapy or photothermal therapy alone. By decorating SN@AuNSs with transferrin (SN@AuNSs-Tf), they further tested the efficacy of targeted thermo-chemotherapy for breast carcinoma [10]. Under NIR laser exposure, MCF-7 breast tumors in mice presented complete regression with the combination of selective targeting, photothermal therapy, and chemotherapy. It is worth noting that both SN@AuNSs and SN@AuNSs-Tf could be excreted from the body with a slow clearance rate via feces and urine, though the diameter of SN@AuNSs was around 130 nm. Additionally, hollow gold nanoshells have been intensively explored for drug delivery and photothermal ablation of tumors by Li's group [12, 19, 52, 162, 163]. In 2012, they demonstrated that hollow nanoshells could be used for

in vivo anticancer drug delivery, which exhibited effective synergistic tumor suppression capability when combined with the NIR light irradiation. Further studies indicated that hollow nanoshells, after being conjugated with a peptide targeting EphB4 overexpressed on the membrane of multiple types of cancer cells, exhibited an improved cellular uptake for three EphB4-positive tumors both in vitro and in vivo. The improved tumor accumulation of peptide-conjugated hollow nanoshells and NIR-trigged release of DOX ultimately contributed to an effective synergistic therapeutic effect on EphB4-positive tumors.

Gold nanorods with strong NIR absorbance and suitable surface modifications have also been widely explored for the combined photothermal and chemotherapy of cancer. One commonly used nanoplatform is mesoporous silica-coated gold nanorods, which have been widely studied for drug delivery and exhibit high drug loading capacity attributed to their mesoporous silica shell. In 2012, Chen's group fabricated mesoporous silica-coated gold nanorods for DOX delivery, observing a precisely NIR light-controllable drug release profile. It was demonstrated that the DOX-loaded mesoporous silica nanorods could offer a synergistic therapeutic effect on A549 cancer cells by utilizing a 790 nm laser irradiation [11]. In another work, Qu's group demonstrated that folic acid-conjugated mesoporous silica-coated gold nanorods with PEGylation after being loaded with an anticancer drug could realize a greatly enhanced treatment effect by combining photothermal therapy with chemotherapy [164]. Almost at the same time, a similar treatment effect in mice was observed, in which RGD peptide was introduced as the targeting moiety to realize a targeted synergistic therapeutic effect in a mouse tumor model [165].

In addition to the mesoporous silica layer incorporation method, a number of different NIR-responsive drug-delivery systems by coating gold nanoparticles with other thermal-responsive materials such as DNA or polymers have been developed. Among them, the most well known is based on gold nanocages, which was constructed by coating nanocages with thermosensitive polymers poly(*N-isopropylacrylamide-co*-acrylamide) (pNIPAAm-*co*-pAAm) as pore blockers [13]. As the temperature was increased above a certain threshold through NIR laser irradiation, the polymer coating would collapse due to a conformational change, and the pores of the nanocages were exposed, which allowed effectors preloaded in the interior to be released (Fig. 2.16). In 2012, Xiao and coworkers assembled DNA duplex strands, which consisted of sequential CG base pairs providing loading sites for DOX, onto gold nanorods [166]. Upon NIR laser illumination, DOX molecules were released at the target site for chemotherapy. The in vivo results showed that the DNA-based platform effectively inhibited tumor through thermo-chemotherapy upon NIR laser irradiation after intratumoral injection. Very recently, Chen et al. successfully coupled photothermal properties and thermoresponsive properties in a single nanocomposite by coating nanorods with a thermoresponsive polymer shell consisting mainly of poly(*N*-isopropylacrylamide-*co*-acrylic acid) [167]. Then, DOX was loaded into the nanocomposite through electrostatic interactions with high loading content up to 24 %. The activation mechanism was thus transformed from heat to NIR laser, which can be used to control the size as well as drug release. A synergistic efficacy of photothermal therapy and chemotherapy was

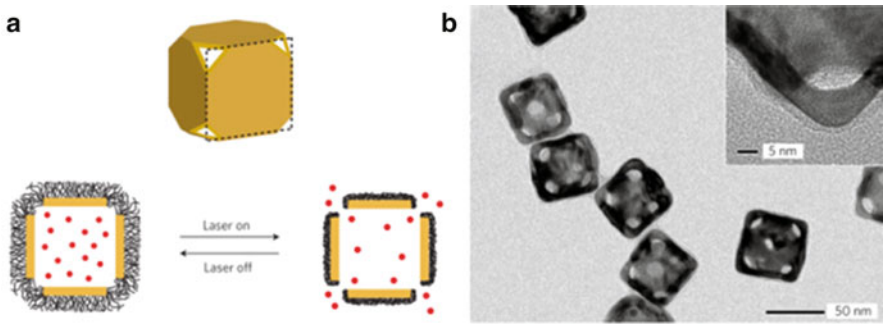

Fig. 2.16 (**a**) Schematic illustration of the controlled-release system. (**b**) TEM images of gold nanocages covered by a pNIPAAm-*co*-pAAm copolymer. The inset shows a magnified TEM image of the corner of such a nanocage (Reprinted by permission from Macmillan Publishers Ltd: Ref. [13], copyright 2009)

observed with complete tumor inhibiting by NIR laser irradiation-induced temperature increase and the released drug, showing very promising potentials for cancer treatments.

2.5 Gold Nanostructures for Diagnostics

As described above, plasmonic gold nanostructures exhibit significantly enhanced radiative properties compared with bulk gold (i.e., light absorption, scattering, and fluorescence). While electromagnetic field enhancement has been widely used in SERS, absorption, and scattering endow gold nanostructures with potentials as multimodal imaging agents [95]. Here we will outline several main modalities for bioimaging based on the intrinsic properties of gold nanostructures, including dark-field imaging, optical coherence tomography, fluorescence imaging, photoacoustic imaging, computed tomography, and SERS-based imaging.

2.5.1 Dark-Field Imaging (DFI)

Gold nanoparticles can strongly scatter light at their plasmon wavelengths, with the scattering cross sections 10^5–10^6 times stronger than that of the emission from a fluorescent dye molecule [122]. Using a simple optical microscope with high-resolution objective lens, light scattered from gold nanostructures can be detected as bright spots even when the size is smaller than the diffraction limit of the microscope. In addition, the light-scattering gold nanoparticles are indefinitely photostable and do not blink, in contrast to conventional fluorophores. These features make gold-based nanoparticle probes very powerful for bioimaging. Sokolov et al. showed

that when gold nanoparticles were conjugated to anti-epidermal growth factor receptor (anti-EGFR) antibodies, they specifically bound to EGFR proteins that are overexpressed on the surfaces of cervical cancer cells [168]. Illumination of the nanoparticle-labeled cells with laser light from either a laser pointer or a confocal microscope lit up the gold nanoparticles and, thus, their associated cancer cells. Later, El-sayed et al. used dark-field optical microscopy to detect gold nanoparticle-labeled cancer cells [169]. The key advantages of DFI are that nanoparticles are imaged in high contrast with true color, making the technique amenable to multiplexed detection schemes by using gold nanoparticles of different sizes and shapes. Furthermore, as demonstrated in 2006 by Huang et al. [46], gold nanorods scatter strongly in the near-infrared region, capable of detecting head and neck cancer cells under excitation at spectral wavelengths where biological tissues exhibit little attenuation. Currently, DFI based on gold nanostructures (spheres, rods, nanocages, and nanoshells) is widely used for cancer imaging through functionalized nanoparticle-receptor binding onto cell surface biomarkers [170–173].

Though highly scattering cross sections of gold nanostructures have been exploited extensively for contrast enhancement in DFI, this diagnostic technique has been limited to in vitro studies. Highly scattering nanostructures of sizes over 100 nm are needed in order to achieve good contrast, which is unsuitable for in vivo blood circulation and accumulation in tumor. Alternatively, a high density of smaller gold nanoparticles can be incubated with cells which upon agglomeration in the cellular environment will increase the effective size and provide enhanced contrast. However, this is also infeasible because of potential toxicity by high-density nanoparticles and its impracticability in vivo. Gold nanostructures with extremely high scattering cross section and small size have not yet been reported. These limitations have prohibited the application of DFI in animal models.

2.5.2 Optical Coherence Tomography

Another imaging modality based on scattering properties is optical coherence tomography (OCT). In OCT, tissue is illuminated with light of coherence, and back-scattering light is detected based on coherence matching between the incident and reflected beams. It can produce three-dimensional images of a subject with micrometer resolution. Since coherence is essential for the detection process, OCT is predominantly sensitive to scattering from tissues rather than absorption. Gold nanostructures resonant at the OCT excitation wavelength have been used as contrast agents due to their ability to produce distinctive backscattered light detectable in highly scattering tissue [174]. In 2007, Halas and coworkers used NIR resonant nanoshells as OCT contrast agents for tumor tissues after their systematical injection [14]. As shown in Fig. 2.17, a significant increase in image contrast from tumor tissue is observed compared with normal tissue or tumor tissue injected with PBS. In another study, gold nanoshells were employed for deep-tissue imaging of rabbit epidermal tissue with high spatial-temporal resolution [175]. Nanoshells enhanced

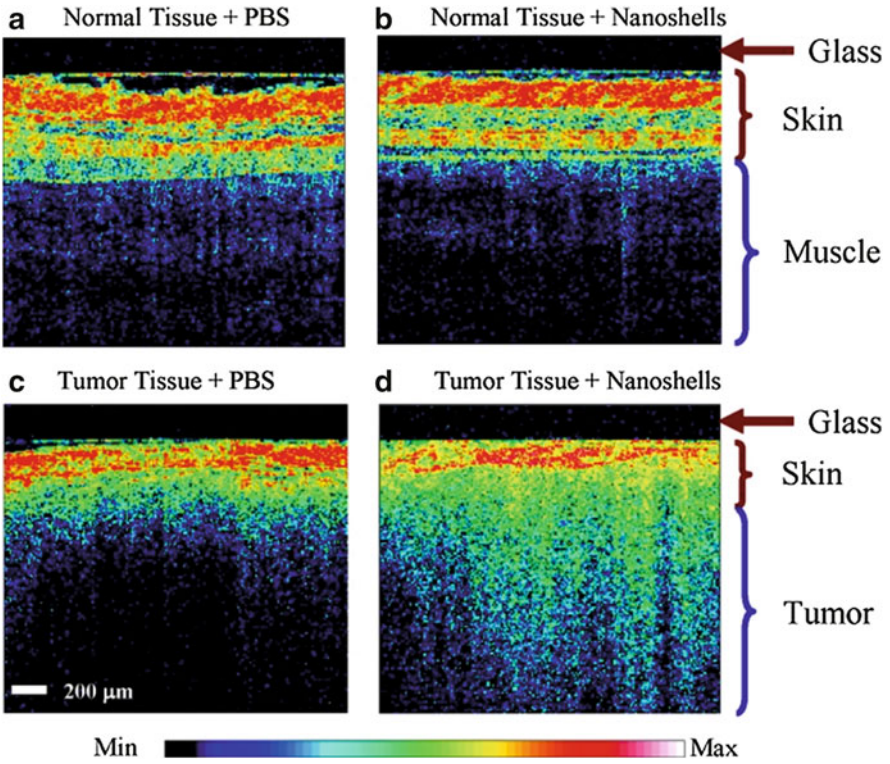

Fig. 2.17 Representative OCT images from normal skin and muscle tissue areas of mice systemically injected with nanoshells (**a**) or with PBS (**b**) and from tumors of mice injected with nanoshells (**c**) or with PBS (**d**) (Reprinted with the permission from Ref. [14]. Copyright 2007 American Chemical Society)

the OCT signal of the different regions of the dermis as well as augmented the contrast of hair follicles and glands in OCT images of skin tissue. In terms of gold nanorods, Oldenburg et al. reported strong OCT contrast at 2 mm depth of human breast tissue with only 10–20 nM of nanorods [176]. OCT signal could only be detected within a few hundred micrometer tissue depth in the control group. In the same year, gold nanoparticles conjugated with anti-EGFR were used to enhance OCT contrast of oral dysplasia in a hamster model in vivo [177]. By using microneedles, the delivery and penetration depth of gold nanoparticles into skin tissue were improved, and clear differences were observed in OCT images between micromorphologies of the carcinogen-treated and untreated epithelial tissues. As a powerful three-dimensional diagnostic tool for real-time imaging without the need to remove specimens, OCT has developed tremendously since its invention [178]. However, due to intense scattering from optically dense tissue, resolutions have remained low, and extensive applications for in vivo cancer imaging, especially deep cancer imaging, merit further investigations.

2.5.3 Two-Photon Luminescence

In comparison to confocal fluorescence microscopy, two-photon luminescence (TPL) has emerged as a powerful tool in the past two decades for cellular imaging and diagnostics, with the advantages of non-bleaching and stable signal, higher spatial resolution, and reduced background signal [179]. Gold nanostructures present enhanced TPL, whose efficiencies can now be improved by simply modifying the geometry [180], making them detectable at single particle levels under femtosecond NIR laser excitation [181, 182]. Durr et al. utilized gold nanorods for TPL imaging of cancer cells embedded in collagen matrixs with 75 μm spatial resolution [183]. The TPL intensity enabled by nanorods was three orders of magnitude brighter than that of two-photon autofluorescence. By using TPL, single-particle tracking of targeted gold nanorods was reported to investigate the mechanisms of cellular uptake [184]. In 2007, He et al. reported the novel detection of circulating tumor cells in vivo using the TPL technique [185]. CTC-mimetic leukemia cells were firstly injected into the blood stream of live mice followed by injection of folate-conjugated gold nanorods to target the CTC in vivo. TPL imaging with an intravital flow cytometer detected single-circulating cells in the vasculature of the mouse ear. Apart from nanorods, other gold nanostructures have also been extensively exploited as TPL contrast agents. The TPL contrast of nanostars functionalized with wheat germ agglutinin was utilized to image their uptake in breast cancer cells as well as nanostars circulating in the vasculature in vivo in mouse models [27]. With nanostars, tissue vasculature was visible under 5 % transmission with minimal background fluorescence, while it required 20 % transmission to observe the vessels without nanostars injected. The feasibility of using nanoshells for single-particle-based in vivo imaging has been validated by Gao et al. [186]. They developed gold nanoshells with plasmon resonance at 800 nm and used them for in vivo blood vessel imaging using two-photon excitation microscopy at an excitation wavelength of 750 nm. They successfully imaged single nanoshell particle in blood vessels and generate optical contrast for blood vessel structure using luminescent signals. Nanocages, nontargeted or targeted, have also been utilized for TPL imaging to probe the dynamical processes of cellular uptake [62, 75].

In particular, due to their large multiphoton absorption capabilities, nanocages have been demonstrated to generate three-photon luminescence (3PL) when excited at 1,290 nm with a femtosecond laser at 4 mW [187]. 3PL exhibited the detection of the distribution of intravenously injected nanocages in the liver of a mouse with minimal autofluorescence from the background and negligible photothermal toxicity. While 3PL contrast agents based on gold nanostructures have not been substantially investigated, these initial results demonstrate the efficacy of this imaging modality and provide a great potential in in vivo diagnostics.

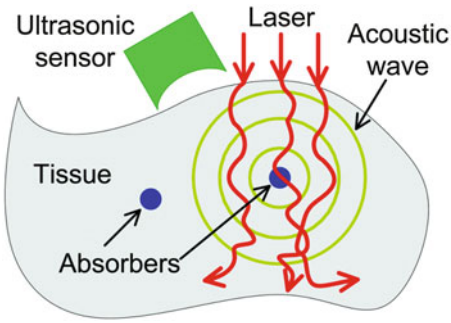

Fig. 2.18 Schematic illustration of laser-induced photoacoustic effect in biological tissue (Reproduced from Ref. [9] by permission of The Royal Society of Chemistry)

2.5.4 Photoacoustic Imaging

Optical imaging, as described previously including DFI, OCT, and TPL, provides rich contrast in biological tissues based on their distinct chemical components. However, the incident photons in tissue, after optical transport mean free path (~1 mm), severely suffer from strong diffusion and thus lose optical coherence and focusing properties. Consequently, the shallow penetration depth of optical imaging in scattering medium fundamentally hampers their application in biomedicine. Nonetheless, photons in tissues can be thermoelastically converted to ultrasonic pressure waves through the photoacoustic (PA) effect, and photoacoustic tomography (PAT) generates images by detecting these ultrasonic waves in tissues. The principle is illustrated in Fig. 2.18 [9]. When a pulsed (or intensity-modulated) laser beam irradiates a biological tissue, a small temperature rise ΔT in the tissue leads to a pressure rise ρ_0 due to thermoelastic expansion that will produce ultrasonic waves. This pressure is given by $\rho_0 = \beta\Delta T/\kappa$, where β is the thermal expansion coefficient and κ is the isothermal compressibility. Theoretically, only 1 mK temperature leap can generate about 800 Pa pressure rise that is far beyond the noise level of a typical ultrasonic transducer [188]. The acoustic pressure, after propagating in the tissue and coupling medium, can be received by an ultrasonic transducer to reconstruct a PA image. By converting the incident photon into ultrasonic emission, PAT can break through the optical diffusion limit in biological tissue, which hybridizes both the merits of rich optical contrast and high ultrasonic resolution, but alleviates their shortcomings in a single modality, permitting anatomical, functional, molecular, and genetic imaging.

Since PA effect is dependent on temperature rise in the tissues, gold nanostructures capable of photothermal heating have great potential as PAT contrast agents in cancer diagnosis. Nearly a decade ago, gold nanostructure-mediated PAT was first realized by gold nanoshells [189]. Three successive injections of nanoshells were administrated to the rat through intravenous injection. The PAT image acquired 20 min after the third administration of contrast agent showed the brain vasculature with enhanced contrast. With the exogenous contrast agent, the optical absorption of blood was increased and the contrast between the vessels and the background tissues was also enhanced. The differential PAT image mapped the exogenous

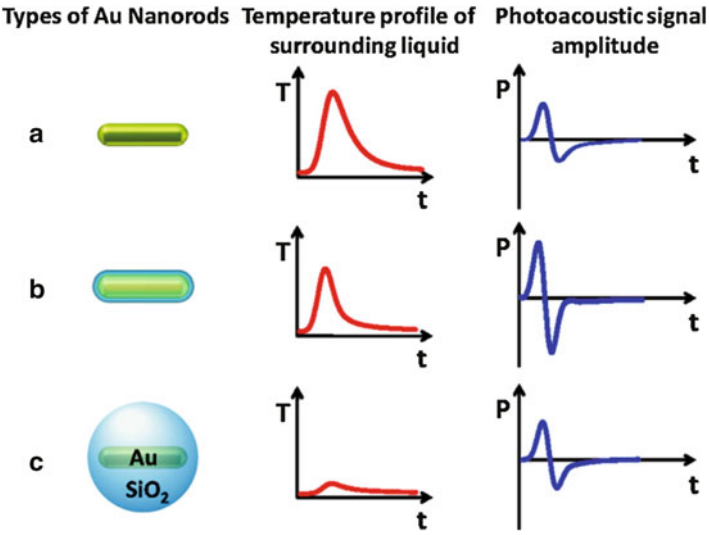

Fig. 2.19 Schematic mechanism of the proposed thermal transport processed from the nanoparticle to the environment and the resulting temporal profiles of the temperature (*T*) near the surface and the amplitude of the photoacoustic signal (*P*) far from the surface of the nanoparticle for (**a**) a bare nanorod, (**b**) a thin silica shell coating nanorod, and (**c**) very thick shell coating nanorod (Reprinted with the permission from Ref. [191]. Copyright 2011 American Chemical Society)

nanoshell distribution in the rat brain. With photothermal conversion efficiency higher than nanoshells, gold nanorods enabled PA signal increasing on a wide variety of ovarian tumor types including 2008, HEY, and SKOV3 cell lines after their intravenous injection [190]. In addition, silica coating of gold nanorods provides a simple method to enhance their performance as contrast agents, producing about threefold higher PA signals than bare nanorods [191, 192]. As shown in Fig. 2.19, silica coating endows nanorods with reduced interfacial resistance and a sharper profile peak and, thus, increased PA signal amplitude. However, silica at a further larger thickness leads to a decrease in the PA signal. Therefore, silica-coated gold nanorods are very promising as a multifunctional platform for enhanced PAT imaging and photothermal therapy of cancer with good photothermal stability, as discussed in the previous section.

Gold nanocages are also excellent contrast agents for PAT, due to the large absorption cross sections [193]. Xia's group demonstrated PAT of cerebral cortex in a rat brain by using nanocages as intravascular contrast agents [194]. A maximum of 80 % PA signal enhancement in the brain cortex was observed after 4 h injection of nanocage solution. In an animal model, sentinel lymph nodes (SLN) containing gold nanocages were identified as deep as 33 mm below the skin surface with good contrast [195]. Nanocage-mediated PAT may potentially eliminate the invasive axillary staging procedures for SLN identification and imaging. In a further study, they investigated nanocages bioconjugated with melanocyte-stimulating hormone in vivo

for molecular PAT of melanomas, and 300 % enhancement was achieved relative to non-conjugated nanocages [196]. Like nanocages, gold nanostars also have great absorption-to-scattering ratio, favorable for photoacoustic imaging. Wang et al. demonstrated that plasmon-resonant gold nanostars could be used with volumetric spectroscopic PAT for noninvasive in vivo mapping of lymphatic systems [197]. In another study, RGD-conjugated gold nanostars targeted the tumor for tumor angiogenesis mapping and monitoring the response of photothermal treatment [198]. Meanwhile, other gold nanostructures with NIR absorption like nanotripods [199] and nanovesicles [151] have also been reported as PAT contrast agents in vivo. All these studies demonstrate the potential of gold nanostructures for contrast enhancement of PAT, and with development of new nanostructures and molecular targeting strategies, the spatiotemporal resolution of PAT can be improved even further.

2.5.5 Computed Tomography

Computed tomography (CT) is one of the most commonly used noninvasive clinical imaging modalities due to its wide availability, high efficiency, and low cost. Owing to the high atomic number ($Z=79$) and k-edge value (80.7 keV), gold nanoparticles generally provide greater contrast than widely used iodinated contrast agents. In addition, X-ray attenuation of gold nanoparticles was not significantly reduced in water or water containing calcium phosphate, in contrast to iodine with contrast effect sensitive to the environment [200]. In 2006, gold nanoparticles with an average size of 1.9 nm from Nanoprobes Inc. were initially studied as X-ray contrast agents [201]. After intravenous injection, in vivo X-ray imaging revealed detailed anatomic structures such as tumors and blood vessels less than 100 μm in diameter. Later, PEGylated gold nanoparticles with diameter of 30 nm were demonstrated to show a high contrast (~2-fold) between hepatoma and normal liver tissue after their intravenous injection into rats [202]. In other studies, gold nanoparticles prepared within the phytochemical gum-arabic (GA) matrix were used as CT contrast agents in pigs, which have physiological and anatomical characteristic similar to those of humans [203, 204]. The GA-gold nanoparticles showed excellent biocompatibility, and significant CT contrast effects were observed at the liver and spleen. The dendrimer-entrapped gold nanoparticles with properties controlled via modification of terminal groups of dendrimers were also successfully used for in vivo blood pool and tumor CT imaging after intravenous injection [205]. With the larger gold nanoparticles entrapped in the dendrimer, greater CT contrast effects could be achieved [206]. In addition to spherical gold nanoparticles, various gold nanostructures can be used as CT contrast agents because the CT contrast effect is not affected by the shape nanoparticles [20, 123, 131].

To acquire information on cellular and molecular processes using CT, contrast agents with targeting ability are required. Tobi Reuveni et al. intravenously injected anti-EGFR-conjugated gold nanoparticles (30 nm) into nude mice implanted with

human squamous cell carcinoma head and neck cancer [207]. The results clearly demonstrated that a small tumor, which was undetectable through anatomical CT, was clearly visible by the molecularly targeted gold nanoparticles. It was further shown that active tumor targeting was more efficient and specific than passive targeting. In another work, gold nanoparticles were modified with glycol chitosan (GC) polymers (GC-Au NPs), which exhibited excellent stability and tumor-targeting ability [208]. Tumor tissue was able to be delineated from the surrounding tissues after 2 h postinjection at high concentration (200 μL, 300 $mgkg^{-1}$). In particular, after 24 h postinjection, the HU value in the tumor tissue increase about fivefold (HU = 254) relative to normal tissue. Furthermore, detailed anatomical information could be acquired from the three-dimensional reconstructed images in which the exact shape of the tumor tissue was clearly visualized. In addition to tumor, gold nanoparticles conjugated with anti-CD4 antibodies were used for in vivo CT studies of peripheral lymph nodes [209]. Larger and targeted nanoparticles showed the highest contrast enhancement compared to nontargeted nanoparticles and smaller nanoparticles because they could deliver more gold atoms.

2.5.6 Surface-Enhanced Raman Scattering (SERS) Based Imaging

Surface-enhanced Raman scattering (SERS) is an ultrasensitive vibrational spectroscopic technique to detect molecules on or near the surface of plasmonic nanostructures, greatly extending the role of standard Raman spectroscopy. Since its discovery in the late 1970s, SERS has been applied to many analyses, especially in biochemistry and life sciences. Particularly, by designing novel nanoprobes named "SERS tags," the past decade has witnessed a plethora of clinical SERS-based studies demonstrating the efficacy of gold nanostructures conjugated with Raman active molecules for molecular imaging in cells and animal model [86]. Raman scattering enhancement of vicinal molecules based on gold nanostructures is primarily attributed to two mechanisms: electromagnetic (EM) and chemical enhancement (CE). EM arises from intense EM fields generated on surface of gold nanoparticles when illuminated at the plasmon resonance. CE is based on dynamical charge transfer where photoexcitation of the metal creates a hot-electron-hole pair which can transfer into the lowest unoccupied molecular orbital of the nearby molecule. The electron subsequently transfers back to the metal with some changed internal molecular vibrations, which gives rise to CE [210, 211]. Together, the two primary mechanisms contribute to the total enhancement. Though eminent progress has been made on SERS-based in vitro bioanalysis [86, 212–216], SERS-based imaging in vivo has yet to reach the status of its counterpart, fluorescence imaging, mainly due to the expensive instrumentation and weak signal of Raman scattering. However, compared with fluorescence imaging as a clinical diagnostic tool, SERS has many advantages including high signal-to-noise ratio, non-photobleaching feature,

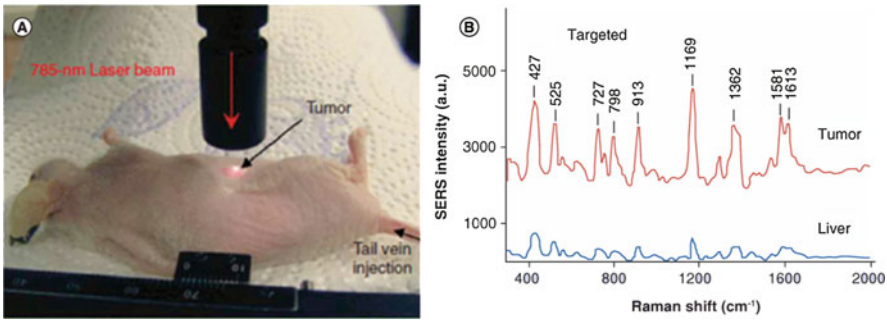

Fig. 2.20 (**a**) Photographs showing a laser beam focusing on the tumor site or on the anatomical location of liver. (**b**) SERS spectra obtained from the tumor and the liver locations by using targeted nanoparticles (Reprinted by permission from Macmillan Publishers Ltd: Ref. [217], copyright 2008)

subpicomolar level sensitivity, excellent multiplexing capability, and single photoexcitation. Owing to these advantages, SERS-based imaging in vivo has aroused increasing attention with some remarkable achievements over the past several years.

Early in 2008, Nie's group investigated SERS-based in vivo tumor targeting using functionalized gold nanoparticles (GNPs) [217]. In this study, diethylthiatricarbocyanine (DTTC), a commercial NIR Raman reporter, was adsorbed onto the surface of 60 nm colloidal GNPs. Then, mixed PEG was applied to conjugate single-chain variable fragment (ScFv) antibodies, which thereby formed targeted SERS nanoprobes. After 5 h of their injection into tumor-bearing mice, clearly distinguished signal intensities were observed on the Raman spectra from targeted nanotags in the tumor region (Fig. 2.20), confirming successful delivery of targeted nanotags to a specific tumor and the capability of noninvasive spectroscopic detection. This highly sensitive technique opens up a new opportunity for the detection of targeting tumors. Then, Park et al. investigated PEGylated Cy7-taged gold nanorods for SERS detection by a passive mechanistic pathway, indicating the clear differentiation between the tumorigenic area and normal skin after their intravenous injection [218]. In 2011, Young-Tae Chang et al. prepared a lipoic acid-containing NIR-active CyNAMLA-381 as a highly sensitive NIR SERS reporter molecule and further applied it to the preparation of ultrasensitive SERS probes for in vivo cancer imaging by conjugating CyNAMLA-381-Au NPs to ScFv anti-HER2 antibodies [219]. Furthermore, Gambhir and coworkers fabricated a unique triple-modality MR-photoacoustic-SERS imaging nanocomposite (termed MPR nanoparticles) to accurately help delineate the margins of brain tumors in living mice both preoperatively and intraoperatively [220]. Specifically, Raman imaging was used for guidance of intraoperative tumor resection. Cancerous foci, not visible to the naked eye, were successfully detected after the tumor resection seems to be completed (Fig. 2.21). Later, they employed SERS probes based on gold nanorods to visualize the margin of ovarian cancer tumors, followed by tumor debulking under guidance of SERS imaging. These two studies highlight the extremely high sensitivity of Raman

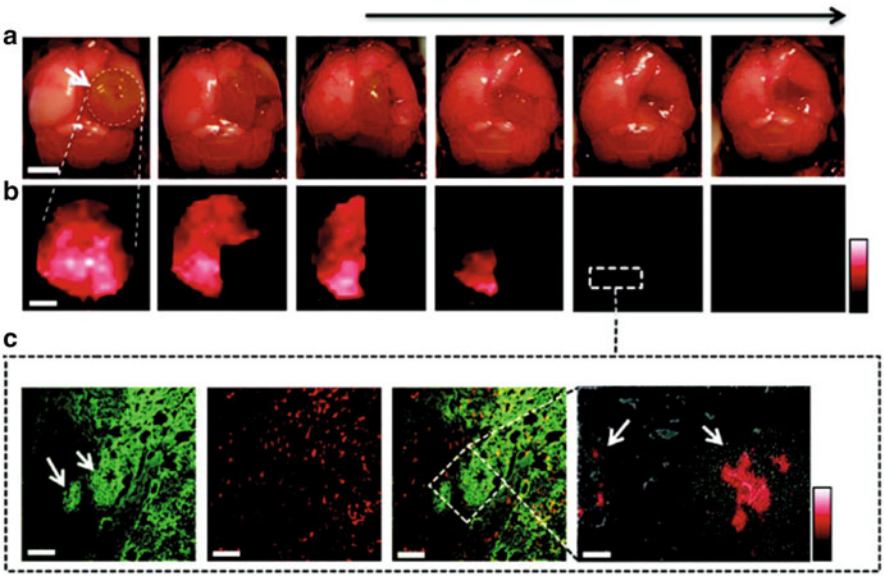

Fig. 2.21 Living tumor-bearing mice underwent craniotomy under general anesthesia. Quarters of the tumor were then sequentially removed as illustrated in the photographs (**a**), and intraoperative Raman imaging was performed after each resection step (**b**) until the entire tumor had been removed, as assessed by visual inspection. After the gross removal of the tumor, several small foci of Raman signal were found in the resection bed. (**c**) A subsequent histological analysis of sections from these foci showed an infiltrative pattern of the tumor in this location, forming finger-like protrusions extending into the surrounding brain tissue. As shown in the Raman microscopy image (*right*), a Raman signal was observed within these protrusions, indicating the selective presence of MPRs. The Raman signal is shown in a linear *red* color scale (Reprinted by permission from Macmillan Publishers Ltd: Ref. [220], copyright 2012)

imaging and open up a new avenue of SERS-tagged gold nanoparticles for clinical translation. More recently, gold-silica SERS nanoparticles combined with a handheld Raman scanner, which is easy to handle in the operating room and allows real-time scanning, to provide SERS image-guided surgical resection of brain tumor was demonstrated, a bigger stride into clinical translation [221].

Specially, multiplexing is the distinctive feature of SERS due to the narrow bandwidths of the vibrational Raman spectra of the reporter molecules. The recent high demand for a sensitive and simultaneous detection of multiple targets in vivo has made SERS technique highly favorable. Gambhir et al. demonstrated multiplexing in vivo with ten different SERS nanotags with distinct spectral characteristics [222, 223]. A mixture of multiple SERS nanotags were administrated intravenously, and their uptake in the liver was imaged 24 h postinjection. Clear distinguishable spectral characteristics were observed in vivo for each individual SERS nanotag at picomolar sensitivity. In another study, molecule-coded gold nanorods as a platform for multiplexed NIR detection were synthesized [224]. It was found that under a NIR excitation source, three unique Raman-coded nanorods might be

distinguished efficiently within ~6 nm of spectral bandwidth, in contrast to ~30 nm of semiconductor quantum dots. Highly sensitive novel NIR Raman reporters, such as Cy7LA, Cy7.5LA, and CyNAMLA-381, were also used to construct SERS nanotags for in vivo multiplexed targeted detection [225]. In addition, Homan Kang et al. developed novel NIR SERS dots consisting of Au/Ag hollow shell assemblies on the surface of silica nanospheres [226]. The signals were detected effectively from deep tissue of up to 8 mm depth and three kinds of NIR SERS dots produce strong SERS signals from deep tissues without spectral overlap after their injection into live animal tissues, demonstrating their potential for in vivo multiplexed detection of specific target molecules. More recently in 2014, "schizophotonic" all-in-one gold nanoparticles were designed by integrating various SERS reporters into biocompatible polymeric surface coating [227]. This technique allows the synthesis of very small (<20 nm) SERS probes, which is crucial for the design of excretable and thus highly translatable imaging agents, and the all-in-one nanoparticles were demonstrated to be capable for multiplexed lymph-node imaging.

SERS imaging has tremendous potentials to deliver accurate diagnosis from the single cell level to subcutaneous tumors. When coupled with other imaging techniques, multimodal SERS can simultaneously achieve high sensitivity and spatial resolution. Gold nanostructures enabled SERS imaging probes from a promising platform for combining SERS imaging with a therapeutic response to generate plasmonic theranostic agents.

2.6 Gold Nanostructures for Imaging-Guided Therapy

To improve the treatment efficiency, combining imaging ability or introducing imaging modalities during therapy within single nanoscale platform, namely, imaging-guided therapy or theranostics, has been proposed. In terms of photothermal theranostics, the exact tumor location, size, and shape should be visualized by imaging initially to ensure that the whole tumor is effectively exposed to the laser during the treatment. Advanced imaging techniques would then allow real-time monitoring of therapeutic responses to achieve optimized efficiency. Nearly a decade ago, before the term theranostics or imaging-guided therapy was coined, the theranostic potential of nanoshells was demonstrated with simultaneous dark-field imaging and photothermal therapy [14, 170, 174]. This was soon followed by the use of nanorods and other core-shell nanostructures for the imaging and therapy of malignant cells in vitro [46, 228, 229]. The past several years have witnessed a tremendous increase in theranostic agents based on gold nanostructures either by combining a single imaging and therapeutic technique or by integrating dual-modality diagnostics with multiple therapeutic functionalities.

Intrinsically, NIR resonant gold nanostructures are theranostic agents without introducing other imaging or therapeutic modalities. As discussed in the previous sections, gold nanoparticles like nanoshells, nanorods, and nanostars with NIR absorption have been widely used in cancer photothermal therapy. Meanwhile,

imaging capabilities based on these gold nanoparticles have also been demonstrated, such as PAT and CT. For example, hollow gold nanoshells have been shown to generate intense photoacoustic signals and induce efficient photothermal treatment. Li et al. used PAT to assess the intravenous delivery of hollow nanoshells targeted to integrins that are overexpressed in both glioma and angiogenic blood vessels in a mouse model of glioma [113]. Mice were then treated with NIR laser, which elevated tumor temperature by 20.7 °C. It was found that photothermal therapy under PAT guidance significantly prolonged the survival of tumor-bearing mice. Recently, cyclic RGD peptide-conjugated plasmonic gold nanostars (RGD-GNS) were designed to specifically target overexpressed integrin $\alpha_v\beta_3$ on tumor neovasculature [198]. By using RGD-GNS, PA signal was significantly boosted for neovasculature visualization, offering high imaging specificity and nanomolar sensitivity. Furthermore, the high absorption-to-scattering ratio of RGD-GNS in the NIR region allows photothermal ablation to neovessels in tumor by laser irradiation, whose therapeutic effect can be noninvasively monitored by PAT. Thus, combining PAT with RGD-GNS makes it possible to image and inhibit tumor angiogenesis and monitor the tumor response in one "on-spot" theranostic platform.

Though gold nanostructures with NIR absorption are greatly promising as theranostic agents, introducing other imaging and therapeutic modalities is nevertheless necessary because of intrinsic drawbacks of these optical imaging methods and single photothermal treatment, as described in Sect. 2.4. Ballistic imaging methods such as OCT, TPL, and SERS suffer from shallow penetration and low spatial resolution, undermining their application in in vivo diagnosis, while for clinical CT, radiation risk is rather a serious concern. As a hybrid imaging modality, PAT manages to break through the optical diffusion limit in biological tissue, but its imaging sensitivity is mainly hampered by surrounding thermal noise and acoustic inherence of the medium itself in the form of black body. Thus, integrating other imaging and therapeutic modalities with advantages compensating for the existing weak points can provide comprehensive information and enable more accurate cancer imaging. In the clinic, magnetic resonance imaging (MRI) is one of the most powerful and noninvasive diagnostic techniques based on the interaction of protons with the surrounding molecules of tissues. MRI can offer high spatial resolution and the capacity to simultaneously obtain physiological and anatomical information. By combining MRI and the above imaging modalities, it is possible to obtain multiple imaging data using the advantages of both methods. Together with therapeutic approaches, gold nanostructures are supposed to find wide applications in imaging-guided therapy.

Recently, Halas group synthesized theranostic nanoshells by encapsulating them in a thin silica epilayer doped with Fe_3O_4 nanoparticles and ICG molecules and targeted HER-2 receptors in breast cancer cells via antibodies [109, 230, 231]. In this design, nanoshells enabled enhancement of ICG quantum yield from ~1 % to nearly ~85 %, and simultaneously, the porous silica layer enabled rapid water diffusion enhancing the MRI relaxivity of the Fe_3O_4 nanoparticles. These theranostic nanoshells provided dual modal MRI and NIR fluorescence imaging capabilities in breast cancer cells in vitro and simultaneous photothermal therapy when excited

with a 200 mW NIR laser overlapping the nanoshell plasmon resonance. The efficacy was also extended in vivo to mouse modals with breast cancer xenografts. Nanoshells were administrated intravenously, and the animals were imaged between 4 and 72 h postinjection. MRI and fluorescence imaging in vivo revealed that the maximum nanoshell accumulation in tumors occurs within 4 h of injection, and within 72 h, nanoshells clear from the tumors to the liver. By using gold-shelled iron oxide nanoclusters, Liu et al. designed a multimodal imaging-guided, magnetic targeting-enhanced photothermal ablation cancer treatment strategy [232]. Such nanocomposites after intravenous injection could be effectively attracted to the tumor, nearby which an external magnetic field was applied. Under the guidance of MRI and PAT, photothermal ablation with excellent therapeutic outcomes (100 % of tumor elimination after NIR laser treatment) was achieved in our animal experiments. In another study, ultrasmall superparamagnetic Fe_3O_4 nanoparticles were adsorbed on the surface of NaYF4-based upconversion nanoparticles, on top of which thin gold shells were formed by seed-mediated reduction growth [233]. The multifunctional nanoparticles were successfully used for in vivo MR and upconversion luminescence imaging-guided and magnetically targeted photothermal therapy. Very recently, West et al. tethered gadolinium to NIR resonant nanoshells, imparting high r_1 relaxivity [234]. MRI- and CT-based modalities with gadolinium-nanoshell enhancement could be used to initially identify suspicious lesions within tissue. Afterwards, optical imaging including OCT and TPL with low-power NIR light could then be performed within appropriate fields of view to obtain molecular information regarding disease state. Finally, under the guidance of the multimodal imaging, NIR laser could be applied site specifically to locally ablate tumor. This class of core-shell nanoparticles is expected to be an attractive theranostic agent for imaging-guided tumor ablation.

Apart from nanoshells, nanorod-mediated theranostics have also rapidly increased within the past few years. Recently, Chen et al. designed theranostic nanorods coated by a mesoporous silica layer loaded with DOX for simultaneous TPL imaging with dual chemo-photothermal therapy in human lung cancer cells [11]. Maximum DOX release was observed with NIR laser treatment at a low pH (4.5) and solution temperature of 48 °C. A cell viability assay clearly indicated that enhanced therapeutic capability was achieved with dual treatment mechanisms rather than hyperthermia or chemotherapy. In another work, He's group developed silica-coated gold nanorods with an additional layer of PEG and loaded the two layers with 3,3′-diethylthiatricarbocyanine iodide (DTTC) and protoporphyrin IX (PpIX), a photosensitizer molecule [235]. The multifunctional nanorods successfully demonstrated diagnosis via SERS and fluorescence imaging in vivo in mice-bearing Hela tumors and treatment via photodynamic treatment mediated by PpIX. In 2011, Cui et al. synthesized folic acid-conjugated silica-modified gold nanorods with highly selective targeting, enhanced radiation therapy effects and excellent photothermal treatment effects on the gastric cancer cells, and strong X-ray attenuation for in vivo X-ray/CT imaging. The nanoprobe is claimed to be a promising candidate with excellent imaging and targeting ability for X-ray/CT imaging-guided targeting dual-mode-enhanced radiation and photothermal therapy.

2.7 Concluding Remarks

Because of their unique features and great potential for a variety of biomedical applications, gold nanostructures represent a major achievement in nanotechnology. The synergy of ideal chemical, physical, and optical properties in a single particle is a resounding affirmation of the promise of nanotechnology in general.

Gold nanostructures have opened new frontiers in medicine. As they are biocompatible, optically tunable, and bind to antibodies, nanogold have a great potential as agents for photothermal cancer therapy, as confirmed by their success in multiple animal studies. Clinical trials, spearheaded by gold nanoshells and currently under way, will most likely establish their efficacy for the treatment of human forms of cancer. Gold nanoparticles are also highly suitable for in vivo imaging studies based on their intrinsic optical and physical properties or through introducing other imaging modalities, with the added benefit of serving as agents for cancer therapy. Likewise, because they accumulate within tumors due to passive and active mechanisms, they hold great promise for revolutionizing cancer detection and therapy.

However, there are several problems, which are yet to be investigated. One of the most important issues is the potential long-term safety concerns of the gold nanoparticles since they are not biodegradable and would retain inside the body for long periods after administration. Another major challenge both in phototherapy and optical imaging is the limited light (even NIR light) penetration depth of no deeper than 1 cm, a great obstacle for tumors located deeply inside the body. Other basic mechanism questions like the response of immune system to photothermal treatment and tumor residues after photothermal ablation merit further investigation. It is hoped that, in the near future, these problems will be addressed and the novel properties of gold nanostructures will continue to be exploited in a growing number of applications. Clearly, it will be very exciting to see many existing applications make the successful transition from the laboratory bench to the clinic.

References

1. Dreaden EC, Alkilany AM, Huang X, Murphy CJ, El-Sayed MA (2012) The golden age: gold nanoparticles for biomedicine. Chem Soc Rev 41(7):2740–2779
2. Schuller JA, Barnard ES, Cai W, Jun YC, White JS, Brongersma ML (2010) Plasmonics for extreme light concentration and manipulation. Nat Mater 9(3):193–204
3. Grzelczak M, Perez-Juste J, Mulvaney P, Liz-Marzan LM (2008) Shape control in gold nanoparticle synthesis. Chem Soc Rev 37(9):1783–1791
4. Boisselier E, Astruc D (2009) Gold nanoparticles in nanomedicine: preparations, imaging, diagnostics, therapies and toxicity. Chem Soc Rev 38(6):1759–1782
5. Torchilin VP (2006) Multifunctional nanocarriers. Adv Drug Deliv Rev 58(14):1532–1555
6. Schneider GF, Subr V, Ulbrich K, Decher G (2009) Multifunctional cytotoxic stealth nanoparticles. A model approach with potential for cancer therapy. Nano Lett 9(2):636–642
7. Alkilany AM, Nagaria PK, Hexel CR, Shaw TJ, Murphy CJ, Wyatt MD (2009) Cellular uptake and cytotoxicity of gold nanorods: molecular origin of cytotoxicity and surface effects. Small 5(6):701–708

8. Qin Z, Bischof JC (2012) Thermophysical and biological responses of gold nanoparticle laser heating. Chem Soc Rev 41(3):1191–1217
9. Nie L, Chen X (2014) Structural and functional photoacoustic molecular tomography aided by emerging contrast agents. Chem Soc Rev 43(20):7132–7170
10. Liu H, Liu T, Wu X, Li L, Tan L, Chen D, Tang F (2012) Targeting gold nanoshells on silica nanorattles: a drug cocktail to fight breast tumors via a single irradiation with near-infrared laser light. Adv Mater 24(6):755–761
11. Zhang Z, Wang L, Wang J, Jiang X, Li X, Hu Z, Ji Y, Wu X, Chen C (2012) Mesoporous silica-coated gold nanorods as a light-mediated multifunctional theranostic platform for cancer treatment. Adv Mater 24(11):1418–1423
12. You J, Zhang R, Xiong C, Zhong M, Melancon M, Gupta S, Nick AM, Sood AK, Li C (2012) Effective photothermal chemotherapy using doxorubicin-loaded gold nanospheres that target EphB4 receptors in tumors. Cancer Res 72(18):4777–4786
13. Yavuz MS, Cheng Y, Chen J, Cobley CM, Zhang Q, Rycenga M, Xie J, Kim C, Song KH, Schwartz AG, Wang LV, Xia Y (2009) Gold nanocages covered by smart polymers for controlled release with near-infrared light. Nat Mater 8(12):935–939
14. Gobin AM, Lee MH, Halas NJ, James WD, Drezek RA, West JL (2007) Near-infrared resonant nanoshells for combined optical imaging and photothermal cancer therapy. Nano Lett 7(7):1929–1934
15. Webb JA, Bardhan R (2014) Emerging advances in nanomedicine with engineered gold nanostructures. Nanoscale 6(5):2502–2530
16. Giannini V, Fernández-Domínguez AI, Heck SC, Maier SA (2011) Plasmonic nanoantennas: fundamentals and their use in controlling the radiative properties of nanoemitters. Chem Rev 111(6):3888–3912
17. Jaque D, Martinez Maestro L, del Rosal B, Haro-Gonzalez P, Benayas A, Plaza JL, Martin Rodriguez E, Garcia Sole J (2014) Nanoparticles for photothermal therapies. Nanoscale 6(16):9494–9530
18. Dong W, Li Y, Niu D, Ma Z, Liu X, Gu J, Zhao W, Zheng Y, Shi J (2013) A simple route to prepare monodisperse Au NP-decorated, dye-doped, superparamagnetic nanocomposites for optical, MR, and CT trimodal imaging. Small 9(15):2500–2508
19. Melancon MP, Lu W, Yang Z, Zhang R, Cheng Z, Elliot AM, Stafford J, Olson T, Zhang JZ, Li C (2008) In vitro and in vivo targeting of hollow gold nanoshells directed at epidermal growth factor receptor for photothermal ablation therapy. Mol Cancer Ther 7(6):1730–1739
20. Popovtzer R, Agrawal A, Kotov NA, Popovtzer A, Balter J, Carey TE, Kopelman R (2008) Targeted gold nanoparticles enable molecular CT imaging of cancer. Nano Lett 8(12):4593–4596
21. Samanta A, Jana S, Das RK, Chang YT (2014) Biocompatible surface-enhanced Raman scattering nanotags for in vivo cancer detection. Nanomedicine (Lond) 9(3):523–535
22. Jain PK, Huang X, El-Sayed IH, El-Sayed MA (2008) Noble metals on the nanoscale: optical and photothermal properties and some applications in imaging, sensing, biology, and medicine. Acc Chem Res 41(12):1578–1586
23. Huang X, Neretina S, El-Sayed MA (2009) Gold nanorods: from synthesis and properties to biological and biomedical applications. Adv Mater 21(48):4880–4910
24. Halas NJ, Lal S, Chang W-S, Link S, Nordlander P (2011) Plasmons in strongly coupled metallic nanostructures. Chem Rev 111(6):3913–3961
25. Weissleder R (2001) A clearer vision for in vivo imaging. Nat Biotechnol 19(4):316–317
26. Smith AM, Mancini MC, Nie S (2009) Bioimaging: second window for in vivo imaging. Nat Nanotechnol 4(11):710–711
27. Hsiangkuo Y, Christopher GK, Hanjun H, Christy MW, Gerald AG, Tuan V-D (2012) Gold nanostars: surfactant-free synthesis, 3D modelling, and two-photon photoluminescence imaging. Nanotechnology 23(7):075102
28. Zhu J, Yong KT, Roy I, Hu R, Ding H, Zhao LL, Swihart MT, He GS, Cui YP, Prasad PN (2010) Additive controlled synthesis of gold nanorods (GNRs) for two-photon luminescence imaging of cancer cells. Nanotechnology 21(28):8

29. Skrabalak SE, Au L, Li X, Xia Y (2007) Facile synthesis of Ag nanocubes and Au nanocages. Nat Protoc 2(9):2182–2190
30. Oldenburg SJ, Averitt RD, Westcott SL, Halas NJ (1998) Nanoengineering of optical resonances. Chem Phys Lett 288(2–4):243–247
31. Shimizu T, Teranishi T, Hasegawa S, Miyake M (2003) Size evolution of alkanethiol-protected gold nanoparticles by heat treatment in the solid state. J Phys Chem B 107(12):2719–2724
32. Ye X, Jin L, Caglayan H, Chen J, Xing G, Zheng C, Doan-Nguyen V, Kang Y, Engheta N, Kagan CR, Murray CB (2012) Improved size-tunable synthesis of monodisperse gold nanorods through the use of aromatic additives. ACS Nano 6(3):2804–2817
33. Pandian Senthil K, Isabel P-S, Benito R-G, JGd Abajo F, Luis ML-M (2008) High-yield synthesis and optical response of gold nanostars. Nanotechnology 19(1):015606
34. Lu X, Au L, McLellan J, Li Z-Y, Marquez M, Xia Y (2007) Fabrication of cubic nanocages and nanoframes by dealloying Au/Ag alloy nanoboxes with an aqueous etchant based on Fe(NO3)3 or NH4OH. Nano Lett 7(6):1764–1769
35. Sonnichsen C, Reinhard BM, Liphardt J, Alivisatos AP (2005) A molecular ruler based on plasmon coupling of single gold and silver nanoparticles. Nat Biotechnol 23(6):741–745
36. Jain PK, Huang W, El-Sayed MA (2007) On the universal scaling behavior of the distance decay of plasmon coupling in metal nanoparticle pairs: a plasmon ruler equation. Nano Lett 7(7):2080–2088
37. Guo L, Xu Y, Ferhan AR, Chen G, Kim D-H (2013) Oriented gold nanoparticle aggregation for colorimetric sensors with surprisingly high analytical figures of merit. J Am Chem Soc 135(33):12338–12345
38. Xia F, Zuo X, Yang R, Xiao Y, Kang D, Vallee-Belisle A, Gong X, Yuen JD, Hsu BB, Heeger AJ, Plaxco KW (2010) Colorimetric detection of DNA, small molecules, proteins, and ions using unmodified gold nanoparticles and conjugated polyelectrolytes. Proc Natl Acad Sci U S A 107(24):10837–10841
39. Chen JIL, Chen Y, Ginger DS (2010) Plasmonic nanoparticle dimers for optical sensing of DNA in complex media. J Am Chem Soc 132(28):9600–9601
40. Anker JN, Hall WP, Lyandres O, Shah NC, Zhao J, Van Duyne RP (2008) Biosensing with plasmonic nanosensors. Nat Mater 7(6):442–453
41. Lim D-K, Jeon K-S, Kim HM, Nam J-M, Suh YD (2010) Nanogap-engineerable Raman-active nanodumbbells for single-molecule detection. Nat Mater 9(1):60–67
42. Nam J, Won N, Jin H, Chung H, Kim S (2009) pH-induced aggregation of gold nanoparticles for photothermal cancer therapy. J Am Chem Soc 131(38):13639–13645
43. Indrasekara AS, Paladini BJ, Naczynski DJ, Starovoytov V, Moghe PV, Fabris L (2013) Dimeric gold nanoparticle assemblies as tags for SERS-based cancer detection. Adv Healthc Mater 2(10):1370–1376
44. Lukianova-Hleb EY, Anderson LJE, Lee S, Hafner JH, Lapotko DO (2010) Hot plasmonic interactions: a new look at the photothermal efficacy of gold nanoparticles. Phys Chem Chem Phys 12(38):12237–12244
45. Hirsch LR, Stafford RJ, Bankson JA, Sershen SR, Rivera B, Price RE, Hazle JD, Halas NJ, West JL (2003) Nanoshell-mediated near-infrared thermal therapy of tumors under magnetic resonance guidance. Proc Natl Acad Sci U S A 100(23):13549–13554
46. Huang X, El-Sayed IH, Qian W, El-Sayed MA (2006) Cancer cell imaging and photothermal therapy in the near-infrared region by using gold nanorods. J Am Chem Soc 128(6):2115–2120
47. Chen J, Wang D, Xi J, Au L, Siekkinen A, Warsen A, Li Z-Y, Zhang H, Xia Y, Li X (2007) Immuno gold nanocages with tailored optical properties for targeted photothermal destruction of cancer cells. Nano Lett 7(5):1318–1322
48. Wang Y, Black KC, Luehmann H, Li W, Zhang Y, Cai X, Wan D, Liu SY, Li M, Kim P, Li ZY, Wang LV, Liu Y, Xia Y (2013) Comparison study of gold nanohexapods, nanorods, and nanocages for photothermal cancer treatment. ACS Nano 7(3):2068–2077

49. Chen C-C, Lin Y-P, Wang C-W, Tzeng H-C, Wu C-H, Chen Y-C, Chen C-P, Chen L-C, Wu Y-C (2006) DNA–gold nanorod conjugates for remote control of localized gene expression by near infrared irradiation. J Am Chem Soc 128(11):3709–3715
50. Jin Y, Gao X (2009) Spectrally tunable leakage-free gold nanocontainers. J Am Chem Soc 131(49):17774–17776
51. Huschka R, Barhoumi A, Liu Q, Roth JA, Ji L, Halas NJ (2012) Gene silencing by gold nanoshell-mediated delivery and laser-triggered release of antisense oligonucleotide and siRNA. ACS Nano 6(9):7681–7691
52. You J, Zhang G, Li C (2010) Exceptionally high payload of doxorubicin in hollow gold nanospheres for near-infrared light-triggered drug release. ACS Nano 4(2):1033–1041
53. Liu Y, Chang Z, Yuan H, Fales AM, Vo-Dinh T (2013) Quintuple-modality (SERS-MRI-CT-TPL-PTT) plasmonic nanoprobe for theranostics. Nanoscale 5(24):12126–12131
54. Link S, Ei-Sayed MA (2003) Optical properties and ultrafast dynamics of metallic nanocrystals. Annu Rev Phys Chem 54:331–366
55. Link S, El-Sayed MA (2000) Shape and size dependence of radiative, non-radiative and photothermal properties of gold nanocrystals. Int Rev Phys Chem 19(3):409–453
56. Link S, Burda C, Mohamed MB, Nikoobakht B, El-Sayed MA (1999) Laser photothermal melting and fragmentation of gold nanorods: energy and laser pulse-width dependence. J Phys Chem A 103(9):1165–1170
57. Tong L, Wei Q, Wei A, Cheng J-X (2009) Gold nanorods as contrast agents for biological imaging: optical properties, surface conjugation and photothermal effects†. Photochem Photobiol 85(1):21–32
58. Yuan H, Fales AM, Vo-Dinh T (2012) TAT peptide-functionalized gold nanostars: enhanced intracellular delivery and efficient NIR photothermal therapy using ultralow irradiance. J Am Chem Soc 134(28):11358–11361
59. Yuan H, Khoury CG, Wilson CM, Grant GA, Bennett AJ, Vo-Dinh T (2012) In vivo particle tracking and photothermal ablation using plasmon-resonant gold nanostars. Nanomedicine 8(8):1355–1363
60. Zhang Y, Yu J, Birch DJS, Chen Y (2010) Gold nanorods for fluorescence lifetime imaging in biology. J Biomed Opt 15(2):020504, 020504-020503
61. Park J, Estrada A, Schwartz JA, Diagaradjane P, Krishnan S, Dunn AK, Tunnell JW (2010) Intra-organ biodistribution of gold nanoparticles using intrinsic two-photon-induced photoluminescence. Lasers Surg Med 42(7):630–639
62. Wang Y, Xu J, Xia X, Yang M, Vangveravong S, Chen J, Mach RH, Xia Y (2012) SV119-gold nanocage conjugates: a new platform for targeting cancer cellsvia sigma-2 receptors. Nanoscale 4(2):421–424
63. Lewinski N, Colvin V, Drezek R (2008) Cytotoxicity of nanoparticles. Small 4(1):26–49
64. Paciotti GF, Myer L, Weinreich D, Goia D, Pavel N, McLaughlin RE, Tamarkin L (2004) Colloidal gold: a novel nanoparticle vector for tumor directed drug delivery. Drug Deliv 11(3):169–183
65. Love JC, Estroff LA, Kriebel JK, Nuzzo RG, Whitesides GM (2005) Self-assembled monolayers of thiolates on metals as a form of nanotechnology. Chem Rev 105(4):1103–1170
66. Brust M, Walker M, Bethell D, Schiffrin DJ, Whyman R (1994) Synthesis of thiol-derivatised gold nanoparticles in a two-phase liquid-liquid system. J Chem Soc Chem Commun 7:801–802
67. Walter M, Akola J, Lopez-Acevedo O, Jadzinsky PD, Calero G, Ackerson CJ, Whetten RL, Gronbeck H, Hakkinen H (2008) A unified view of ligand-protected gold clusters as superatom complexes. Proc Natl Acad Sci U S A 105(27):9157–9162
68. Martin BR, Dermody DJ, Reiss BD, Fang M, Lyon LA, Natan MJ, Mallouk TE (1999) Orthogonal self-assembly on colloidal gold-platinum nanorods. Adv Mater 11(12):1021–1025
69. Hou W, Dasog M, Scott RWJ (2009) Probing the relative stability of thiolate- and dithiolate-protected Au monolayer-protected clusters. Langmuir 25(22):12954–12961

70. Zhao Y, Pérez-Segarra W, Shi Q, Wei A (2005) Dithiocarbamate assembly on gold. J Am Chem Soc 127(20):7328–7329
71. Daniel M-C, Astruc D (2003) Gold nanoparticles: assembly, supramolecular chemistry, quantum-size-related properties, and applications toward biology, catalysis, and nanotechnology. Chem Rev 104(1):293–346
72. Yee CK, Ulman A, Ruiz JD, Parikh A, White H, Rafailovich M (2003) Alkyl selenide- and alkyl thiolate-functionalized gold nanoparticles: chain packing and bond nature. Langmuir 19(22):9450–9458
73. Schmid G, Pfeil R, Boese R, Bandermann F, Meyer S, Calis GHM, van der Velden JWA (1981) Au55[P(C6H5)3]12CI6 – ein Goldcluster ungewöhnlicher Größe. Chem Ber 114(11):3634–3642
74. Peer D, Karp JM, Hong S, Farokhzad OC, Margalit R, Langer R (2007) Nanocarriers as an emerging platform for cancer therapy. Nat Nanotechnol 2(12):751–760
75. Au L, Zhang Q, Cobley CM, Gidding M, Schwartz AG, Chen J, Xia Y (2009) Quantifying the cellular uptake of antibody-conjugated Au nanocages by two-photon microscopy and inductively coupled plasma mass spectrometry. ACS Nano 4(1):35–42
76. Gittins DI, Caruso F (2001) Tailoring the polyelectrolyte coating of metal nanoparticles. J Phys Chem B 105(29):6846–6852
77. Gole A, Murphy CJ (2005) Polyelectrolyte-coated gold nanorods: synthesis, characterization and immobilization. Chem Mater 17(6):1325–1330
78. Murphy CJ, Thompson LB, Alkilany AM, Sisco PN, Boulos SP, Sivapalan ST, Yang JA, Chernak DJ, Huang J (2010) The many faces of gold nanorods. J Phys Chem Lett 1(19):2867–2875
79. Brown SD, Nativo P, Smith J-A, Stirling D, Edwards PR, Venugopal B, Flint DJ, Plumb JA, Graham D, Wheate NJ (2010) Gold nanoparticles for the improved anticancer drug delivery of the active component of oxaliplatin. J Am Chem Soc 132(13):4678–4684
80. Wong JK, Yip SP, Lee TM (2012) Silica-modified oligonucleotide-gold nanoparticle conjugate enables closed-tube colorimetric polymerase chain reaction. Small 8(2):214–219
81. Wu P, Gao Y, Zhang H, Cai C (2012) Aptamer-guided silver-gold bimetallic nanostructures with highly active surface-enhanced Raman scattering for specific detection and near-infrared photothermal therapy of human breast cancer cells. Anal Chem 84(18):7692–7699
82. Huh YS, Chung AJ, Erickson D (2009) Surface enhanced Raman spectroscopy and its application to molecular and cellular analysis. Microfluid Nanofluid 6(3):285–297
83. Liz-Marzán LM, Giersig M, Mulvaney P (1996) Synthesis of nanosized gold–silica core–shell particles. Langmuir 12(18):4329–4335
84. Jana NR, Earhart C, Ying JY (2007) Synthesis of water-soluble and functionalized nanoparticles by silica coating. Chem Mater 19(21):5074–5082
85. Banholzer MJ, Harris N, Millstone JE, Schatz GC, Mirkin CA (2010) Abnormally large plasmonic shifts in silica-protected gold triangular nanoprisms†. J Phys Chem C 114(16):7521–7526
86. Wang Y, Yan B, Chen L (2013) SERS tags: novel optical nanoprobes for bioanalysis. Chem Rev 113(3):1391–1428
87. Roti Roti JL (2008) Cellular responses to hyperthermia (40–46°C): cell killing and molecular events. Int J Hyperth 24(1):3–15
88. O'Grady NP, Barie PS, Bartlett JG, Bleck T, Garvey G, Jacobi J, Linden P, Maki DG, Nam M, Pasculle W, Pasquale MD, Tribett DL, Masur H (1998) Practice guidelines for evaluating new fever in critically ill adult patients. Clin Infect Dis 26(5):1042–1059
89. Fisher JW, Sarkar S, Buchanan CF, Szot CS, Whitney J, Hatcher HC, Torti SV, Rylander CG, Rylander MN (2010) Photothermal response of human and murine cancer cells to multiwalled carbon nanotubes after laser irradiation. Cancer Res 70(23):9855–9864
90. Hildebrandt B, Wust P, Ahlers O, Dieing A, Sreenivasa G, Kerner T, Felix R, Riess H (2002) The cellular and molecular basis of hyperthermia. Crit Rev Oncol Hematol 43(1):33–56

91. Habash RW, Bansal R, Krewski D, Alhafid HT (2007) Thermal therapy, part IV: electromagnetic and thermal dosimetry. Crit Rev Biomed Eng 35(1–2):123–182
92. Chicheł A, Skowronek J, Kubaszewska M, Kanikowski M (2007) Hyperthermia – description of a method and a review of clinical applications. Rep Pract Oncol Radiother 12(5):267–275
93. Pissuwan D, Valenzuela SM, Cortie MB (2006) Therapeutic possibilities of plasmonically heated gold nanoparticles. Trends Biotechnol 24(2):62–67
94. Kennedy LC, Bickford LR, Lewinski NA, Coughlin AJ, Hu Y, Day ES, West JL, Drezek RA (2011) A New Era for cancer treatment: gold-nanoparticle-mediated thermal therapies. Small 7(2):169–183
95. Dreaden EC, Mackey MA, Huang X, Kang B, El-Sayed MA (2011) Beating cancer in multiple ways using nanogold. Chem Soc Rev 40(7):3391–3404
96. Cheng L, Wang C, Feng L, Yang K, Liu Z (2014) Functional nanomaterials for phototherapies of cancer. Chem Rev 114(21):10869–10939
97. Caccamo AE, Desenzani S, Belloni L, Borghetti AF, Bettuzzi S (2006) Nuclear clusterin accumulation during heat shock response: implications for cell survival and thermo-tolerance induction in immortalized and prostate cancer cells. J Cell Physiol 207(1):208–219
98. Bardhan R, Lal S, Joshi A, Halas NJ (2011) Theranostic nanoshells: from probe design to imaging and treatment of cancer. Acc Chem Res 44(10):936–946
99. Melancon MP, Zhou M, Li C (2011) Cancer theranostics with near-infrared light-activatable multimodal nanoparticles. Acc Chem Res 44(10):947–956
100. Zhang Z, Wang J, Chen C (2013) Near-infrared light-mediated nanoplatforms for cancer thermo-chemotherapy and optical imaging. Adv Mater 25(28):3869–3880
101. Matsushita-Ishiodori Y, Ohtsuki T (2012) Photoinduced RNA interference. Acc Chem Res 45(7):1039–1047
102. Chen W, Carubelli R, Liu H, Nordquist R (2003) Laser immunotherapy. Mol Biotechnol 25(1):37–43
103. Phonthammachai N, Kah JCY, Jun G, Sheppard CJR, Olivo MC, Mhaisalkar SG, White TJ (2008) Synthesis of contiguous silica–gold core–shell structures: critical parameters and processes. Langmuir 24(9):5109–5112
104. Brinson BE, Lassiter JB, Levin CS, Bardhan R, Mirin N, Halas NJ (2008) Nanoshells made easy: improving Au layer growth on nanoparticle surfaces. Langmuir 24(24):14166–14171
105. Lal S, Clare SE, Halas NJ (2008) Nanoshell-enabled photothermal cancer therapy: impending clinical impact. Acc Chem Res 41(12):1842–1851
106. O'Neal DP, Hirsch LR, Halas NJ, Payne JD, West JL (2004) Photo-thermal tumor ablation in mice using near infrared-absorbing nanoparticles. Cancer Lett 209(2):171–176
107. Huiyu L, Dong C, Fangqiong T, Gangjun D, Linlin L, Xianwei M, Wei L, Yangde Z, Xu T, Yi L (2008) Photothermal therapy of Lewis lung carcinoma in mice using gold nanoshells on carboxylated polystyrene spheres. Nanotechnology 19(45):455101
108. Liu H, Chen D, Li L, Liu T, Tan L, Wu X, Tang F (2011) Multifunctional gold nanoshells on silica nanorattles: a platform for the combination of photothermal therapy and chemotherapy with low systemic toxicity. Angew Chem Int Ed 50(4):891–895
109. Bardhan R, Chen W, Bartels M, Perez-Torres C, Botero MF, McAninch RW, Contreras A, Schiff R, Pautler RG, Halas NJ, Joshi A (2010) Tracking of multimodal therapeutic nanocomplexes targeting breast cancer in vivo. Nano Lett 10(12):4920–4928
110. Ma Y, Liang X, Tong S, Bao G, Ren Q, Dai Z (2013) Gold nanoshell nanomicelles for potential magnetic resonance imaging, light-triggered drug release, and photothermal therapy. Adv Funct Mater 23(7):815–822
111. Dong W, Li Y, Niu D, Ma Z, Gu J, Chen Y, Zhao W, Liu X, Liu C, Shi J (2011) Facile synthesis of monodisperse superparamagnetic Fe3O4 Core@hybrid@Au shell nanocomposite for bimodal imaging and photothermal therapy. Adv Mater 23(45):5392–5397
112. Lu W, Xiong C, Zhang G, Huang Q, Zhang R, Zhang JZ, Li C (2009) Targeted photothermal ablation of murine melanomas with melanocyte-stimulating hormone analog–conjugated hollow gold nanospheres. Clin Cancer Res 15(3):876–886

113. Lu W, Melancon MP, Xiong C, Huang Q, Elliott A, Song S, Zhang R, Flores LG, Gelovani JG, Wang LV, Ku G, Stafford RJ, Li C (2011) Effects of photoacoustic imaging and photothermal ablation therapy mediated by targeted hollow gold nanospheres in an orthotopic mouse xenograft model of glioma. Cancer Res 71(19):6116–6121
114. Cole JR, Mirin NA, Knight MW, Goodrich GP, Halas NJ (2009) Photothermal efficiencies of nanoshells and nanorods for clinical therapeutic applications. J Phys Chem C 113(28):12090–12094
115. Jain PK, El-Sayed IH, El-Sayed MA (2007) Au nanoparticles target cancer. Nano Today 2(1):18–29
116. Bardhan R, Mukherjee S, Mirin NA, Levit SD, Nordlander P, Halas NJ (2010) Nanosphere-in-a-nanoshell: a simple nanomatryushka†. J Phys Chem C 114(16):7378–7383
117. Ayala-Orozco C, Urban C, Knight MW, Urban AS, Neumann O, Bishnoi SW, Mukherjee S, Goodman AM, Charron H, Mitchell T, Shea M, Roy R, Nanda S, Schiff R, Halas NJ, Joshi A (2014) Au nanomatryoshkas as efficient near-infrared photothermal transducers for cancer treatment: benchmarking against nanoshells. ACS Nano 8(6):6372–6381
118. Ayala-Orozco C, Urban C, Bishnoi S, Urban A, Charron H, Mitchell T, Shea M, Nanda S, Schiff R, Halas N, Joshi A (2014) Sub-100nm gold nanomatryoshkas improve photo-thermal therapy efficacy in large and highly aggressive triple negative breast tumors. J Control Release 191:90–97
119. Gao Y, Li Y, Wang Y, Chen Y, Gu J, Zhao W, Ding J, Shi J (2014) Controlled synthesis of multilayered gold nanoshells for enhanced photothermal therapy and SERS detection. Small 11(1):77–83
120. Jorden D, Goodrich GP, Schwartz J, Halas NJ, West J (2012) Nanospectra biosciences. http://www.nanospectra.com/index.html
121. Nikoobakht B, El-Sayed MA (2003) Preparation and growth mechanism of gold nanorods (NRs) using seed-mediated growth method. Chem Mater 15(10):1957–1962
122. Jain PK, Lee KS, El-Sayed IH, El-Sayed MA (2006) Calculated absorption and scattering properties of gold nanoparticles of different size, shape, and composition: applications in biological imaging and biomedicine. J Phys Chem B 110(14):7238–7248
123. von Maltzahn G, Park J-H, Agrawal A, Bandaru NK, Das SK, Sailor MJ, Bhatia SN (2009) Computationally guided photothermal tumor therapy using long-circulating gold nanorod antennas. Cancer Res 69(9):3892–3900
124. Dickerson EB, Dreaden EC, Huang X, El-Sayed IH, Chu H, Pushpanketh S, McDonald JF, El-Sayed MA (2008) Gold nanorod assisted near-infrared plasmonic photothermal therapy (PPTT) of squamous cell carcinoma in mice. Cancer Lett 269(1):57–66
125. Choi WI, Kim J-Y, Kang C, Byeon CC, Kim YH, Tae G (2011) Tumor regression in vivo by photothermal therapy based on gold-nanorod-loaded, functional nanocarriers. ACS Nano 5(3):1995–2003
126. Li Z, Huang P, Zhang X, Lin J, Yang S, Liu B, Gao F, Xi P, Ren Q, Cui D (2009) RGD-conjugated dendrimer-modified gold nanorods for in vivo tumor targeting and photothermal therapy†. Mol Pharm 7(1):94–104
127. Horiguchi Y, Honda K, Kato Y, Nakashima N, Niidome Y (2008) Photothermal reshaping of gold nanorods depends on the passivating layers of the nanorod surfaces. Langmuir 24(20):12026–12031
128. Candice LD, Pinhas E, Astrid C-R, Steven LJ, Jeffrey JLC (2009) Depth of photothermal conversion of gold nanorods embedded in a tissue-like phantom. Nanotechnology 20(19):195102
129. Chon JWM, Bullen C, Zijlstra P, Gu M (2007) Spectral encoding on gold nanorods doped in a silica sol–gel matrix and its application to high-density optical data storage. Adv Funct Mater 17(6):875–880
130. Zijlstra P, Chon JWM, Gu M (2007) Effect of heat accumulation on the dynamic range of a gold nanorod dopedpolymer nanocomposite for optical laser writing and patterning. Opt Express 15(19):12151–12160

131. Huang P, Bao L, Zhang C, Lin J, Luo T, Yang D, He M, Li Z, Gao G, Gao B, Fu S, Cui D (2011) Folic acid-conjugated silica-modified gold nanorods for X-ray/CT imaging-guided dual-mode radiation and photo-thermal therapy. Biomaterials 32(36):9796–9809
132. Sun Y, Xia Y (2004) Mechanistic study on the replacement reaction between silver nanostructures and chloroauric acid in aqueous medium. J Am Chem Soc 126(12):3892–3901
133. Chen J, McLellan JM, Siekkinen A, Xiong Y, Li Z-Y, Xia Y (2006) Facile synthesis of gold–silver nanocages with controllable pores on the surface. J Am Chem Soc 128(46):14776–14777
134. Skrabalak SE, Chen J, Sun Y, Lu X, Au L, Cobley CM, Xia Y (2008) Gold nanocages: synthesis, properties, and applications. Acc Chem Res 41(12):1587–1595
135. Chen J, Glaus C, Laforest R, Zhang Q, Yang M, Gidding M, Welch MJ, Xia Y (2010) Gold nanocages as photothermal transducers for cancer treatment. Small 6(7):811–817
136. Sun T, Wang Y, Wang Y, Xu J, Zhao X, Vangveravong S, Mach RH, Xia Y (2014) Using SV119-gold nanocage conjugates to eradicate cancer stem cells through a combination of photothermal and chemo therapies. Adv Healthc Mater 3(8):1283–1291
137. Julien RGN, Delphine M, Frederic L, Nicholas PB, Sophie M, Yann L, Jacqueline M, Frederic C, Guillaume M, Ana-Maria G, Alexis M, Emmanuel C, Patrice LB, Kenji K, Stephane P (2012) Synthesis of PEGylated gold nanostars and bipyramids for intracellular uptake. Nanotechnology 23(46):465602
138. Lu W, Singh AK, Khan SA, Senapati D, Yu H, Ray PC (2010) Gold nano-popcorn-based targeted diagnosis, nanotherapy treatment, and in situ monitoring of photothermal therapy response of prostate cancer cells using surface-enhanced Raman spectroscopy. J Am Chem Soc 132(51):18103–18114
139. Gobin AM, Watkins EM, Quevedo E, Colvin VL, West JL (2010) Near-infrared-resonant gold/gold sulfide nanoparticles as a photothermal cancer therapeutic agent. Small 6(6):745–752
140. Pelaz B, Grazu V, Ibarra A, Magen C, del Pino P, de la Fuente JM (2012) Tailoring the synthesis and heating ability of gold nanoprisms for bioapplications. Langmuir 28(24):8965–8970
141. Tsai MF, Chang SH, Cheng FY, Shanmugam V, Cheng YS, Su CH, Yeh CS (2013) Au nanorod design as light-absorber in the first and second biological near-infrared windows for in vivo photothermal therapy. ACS Nano 7(6):5330–5342
142. Rosenberg SA, Lotze MT, Yang JC, Linehan WM, Seipp C, Calabro S, Karp SE, Sherry RM, Steinberg S, White DE (1989) Combination therapy with interleukin-2 and alpha-interferon for the treatment of patients with advanced cancer. J Clin Oncol 7(12):1863–1874
143. O'Shaughnessy J, Miles D, Vukelja S, Moiseyenko V, Ayoub J-P, Cervantes G, Fumoleau P, Jones S, Lui W-Y, Mauriac L, Twelves C, Van Hazel G, Verma S, Leonard R (2002) Superior survival with capecitabine plus docetaxel combination therapy in anthracycline-pretreated patients with advanced breast cancer: phase III trial results. J Clin Oncol 20(12):2812–2823
144. Coley HM (2008) Mechanisms and strategies to overcome chemotherapy resistance in metastatic breast cancer. Cancer Treat Rev 34(4):378–390
145. Fidler IJ (2003) The pathogenesis of cancer metastasis: the 'seed and soil' hypothesis revisited. Nat Rev Cancer 3(6):453–458
146. Sargent DJ, Wieand HS, Haller DG, Gray R, Benedetti JK, Buyse M, Labianca R, Seitz JF, O'Callaghan CJ, Francini G, Grothey A, O'Connell M, Catalano PJ, Blanke CD, Kerr D, Green E, Wolmark N, Andre T, Goldberg RM, De Gramont A (2005) Disease-free survival versus overall survival as a primary end point for adjuvant colon cancer studies: individual patient data from 20,898 patients on 18 randomized trials. J Clin Oncol 23(34):8664–8670
147. Lee S-M, Kim HJ, Ha Y-J, Park YN, Lee S-K, Park Y-B, Yoo K-H (2012) Targeted chemo-photothermal treatments of rheumatoid arthritis using gold half-shell multifunctional nanoparticles. ACS Nano 7(1):50–57
148. Dougherty TJ, Gomer CJ, Henderson BW, Jori G, Kessel D, Korbelik M, Moan J, Peng Q (1998) Photodynamic therapy. J Natl Cancer Inst 90(12):889–905

149. Jang B, Park J-Y, Tung C-H, Kim I-H, Choi Y (2011) Gold nanorod–photosensitizer complex for near-infrared fluorescence imaging and photodynamic/photothermal therapy in vivo. ACS Nano 5(2):1086–1094
150. Wang J, Zhu G, You M, Song E, Shukoor MI, Zhang K, Altman MB, Chen Y, Zhu Z, Huang CZ, Tan W (2012) Assembly of aptamer switch probes and photosensitizer on gold nanorods for targeted photothermal and photodynamic cancer therapy. ACS Nano 6(6):5070–5077
151. Lin J, Wang S, Huang P, Wang Z, Chen S, Niu G, Li W, He J, Cui D, Lu G, Chen X, Nie Z (2013) Photosensitizer-loaded gold vesicles with strong plasmonic coupling effect for imaging-guided photothermal/photodynamic therapy. ACS Nano 7(6):5320–5329
152. Wang S, Huang P, Nie L, Xing R, Liu D, Wang Z, Lin J, Chen S, Niu G, Lu G, Chen X (2013) Single continuous wave laser induced photodynamic/plasmonic photothermal therapy using photosensitizer-functionalized gold nanostars. Adv Mater 25(22):3055–3061
153. Vijayaraghavan P, Liu CH, Vankayala R, Chiang CS, Hwang KC (2014) Designing multi-branched gold nanoechinus for NIR light activated dual modal photodynamic and photothermal therapy in the second biological window. Adv Mater 26(39):6689–6695
154. Li Y, Wen T, Zhao R, Liu X, Ji T, Wang H, Shi X, Shi J, Wei J, Zhao Y, Wu X, Nie G (2014) Localized electric field of plasmonic nanoplatform enhanced photodynamic tumor therapy. ACS Nano 8(11):11529–11542
155. Min Y, Mao C-Q, Chen S, Ma G, Wang J, Liu Y (2012) Combating the drug resistance of cisplatin using a platinum prodrug based delivery system. Angew Chem Int Ed 51(27):6742–6747
156. May JP, Li S-D (2013) Hyperthermia-induced drug targeting. Expert Opin Drug Deliv 10(4):511–527
157. Hauck TS, Jennings TL, Yatsenko T, Kumaradas JC, Chan WCW (2008) Enhancing the toxicity of cancer chemotherapeutics with gold nanorod hyperthermia. Adv Mater 20(20):3832–3838
158. Ghosh P, Han G, De M, Kim CK, Rotello VM (2008) Gold nanoparticles in delivery applications. Adv Drug Deliv Rev 60(11):1307–1315
159. You J-O, Guo P, Auguste DT (2013) A drug-delivery vehicle combining the targeting and thermal ablation of HER2+ breast-cancer cells with triggered drug release. Angew Chem Int Ed 52(15):4141–4146
160. Nam J, La W-G, Hwang S, Ha YS, Park N, Won N, Jung S, Bhang SH, Ma Y-J, Cho Y-M, Jin M, Han J, Shin J-Y, Wang EK, Kim SG, Cho S-H, Yoo J, Kim B-S, Kim S (2013) pH-responsive assembly of gold nanoparticles and "Spatiotemporally Concerted" drug release for synergistic cancer therapy. ACS Nano 7(4):3388–3402
161. Lee S-M, Park H, Yoo K-H (2010) Synergistic cancer therapeutic effects of locally delivered drug and heat using multifunctional nanoparticles. Adv Mater 22(36):4049–4053
162. You J, Shao R, Wei X, Gupta S, Li C (2010) Near-infrared light triggers release of paclitaxel from biodegradable microspheres: photothermal effect and enhanced antitumor activity. Small 6(9):1022–1031
163. You J, Zhang R, Zhang G, Zhong M, Liu Y, Van Pelt CS, Liang D, Wei W, Sood AK, Li C (2012) Photothermal-chemotherapy with doxorubicin-loaded hollow gold nanospheres: a platform for near-infrared light-trigged drug release. J Control Release 158(2):319–328
164. Yang X, Liu Z, Li Z, Pu F, Ren J, Qu X (2013) Near-infrared-controlled, targeted hydrophobic drug-delivery system for synergistic cancer therapy. Chem Eur J 19(31):10388–10394
165. Shen S, Tang H, Zhang X, Ren J, Pang Z, Wang D, Gao H, Qian Y, Jiang X, Yang W (2013) Targeting mesoporous silica-encapsulated gold nanorods for chemo-photothermal therapy with near-infrared radiation. Biomaterials 34(12):3150–3158
166. Xiao Z, Ji C, Shi J, Pridgen EM, Frieder J, Wu J, Farokhzad OC (2012) DNA self-assembly of targeted near-infrared-responsive gold nanoparticles for cancer thermo-chemotherapy. Angew Chem Int Ed 51(47):11853–11857
167. Zhang Z, Wang J, Nie X, Wen T, Ji Y, Wu X, Zhao Y, Chen C (2014) Near infrared laser-induced targeted cancer therapy using thermoresponsive polymer encapsulated gold nanorods. J Am Chem Soc 136(20):7317–7326

168. Sokolov K, Follen M, Aaron J, Pavlova I, Malpica A, Lotan R, Richards-Kortum R (2003) Real-time vital optical imaging of precancer using anti-epidermal growth factor receptor antibodies conjugated to gold nanoparticles. Cancer Res 63(9):1999–2004
169. El-Sayed IH, Huang X, El-Sayed MA (2005) Surface plasmon resonance scattering and absorption of anti-EGFR antibody conjugated gold nanoparticles in cancer diagnostics: applications in oral cancer. Nano Lett 5(5):829–834
170. Loo C, Lowery A, Halas N, West J, Drezek R (2005) Immunotargeted nanoshells for integrated cancer imaging and therapy. Nano Lett 5(4):709–711
171. Loo C, Hirsch L, Lee M-H, Chang E, West J, Halas N, Drezek R (2005) Gold nanoshell bioconjugates for molecular imaging in living cells. Opt Lett 30(9):1012–1014
172. Ding H, Yong K-T, Roy I, Pudavar HE, Law WC, Bergey EJ, Prasad PN (2007) Gold nanorods coated with multilayer polyelectrolyte as contrast agents for multimodal imaging. J Phys Chem C 111(34):12552–12557
173. Chanda N, Shukla R, Katti KV, Kannan R (2009) Gastrin releasing protein receptor specific gold nanorods: breast and prostate tumor avid nanovectors for molecular imaging. Nano Lett 9(5):1798–1805
174. Loo C, Lin A, Hirsch L, Lee MH, Barton J, Halas NJ, West J, Drezek R (2004) Nanoshell-enabled photonics-based imaging and therapy of cancer. Technol Cancer Res Treat 3(1):33–40
175. Zagaynova EV, Shirmanova MV, Kirillin MY, Khlebtsov BN, Orlova AG, Balalaeva IV, Sirotkina MA, Bugrova ML, Agrba PD, Kamensky VA (2008) Contrasting properties of gold nanoparticles for optical coherence tomography: phantom, in vivo studies and Monte Carlo simulation. Phys Med Biol 53(18):4995
176. Oldenburg AL, Hansen MN, Ralston TS, Wei A, Boppart SA (2009) Imaging gold nanorods in excised human breast carcinoma by spectroscopic optical coherence tomography. J Mater Chem 19(35):6407–6411
177. Kim CS, Wilder-Smith P, Ahn Y-C, Liaw L-HL, Chen Z, Kwon YJ (2009) Enhanced detection of early-stage oral cancer in vivo by optical coherence tomography using multimodal delivery of gold nanoparticles. J Biomed Opt 14(3):034008, 034008-034008
178. Huang D, Swanson E, Lin C, Schuman J, Stinson W, Chang W, Hee M, Flotte T, Gregory K, Puliafito C et al (1991) Optical coherence tomography. Science 254(5035):1178–1181
179. Zhou Y, Wu X, Wang T, Ming T, Wang PN, Zhou LW, Chen JY (2010) A comparison study of detecting gold nanorods in living cells with confocal reflectance microscopy and two-photon fluorescence microscopy. J Microsc 237(2):200–207
180. Jiang Y, Horimoto NN, Imura K, Okamoto H, Matsui K, Shigemoto R (2009) Bioimaging with two-photon-induced luminescence from triangular nanoplates and nanoparticle aggregates of gold. Adv Mater 21(22):2309–2313
181. Wang H, Huff TB, Zweifel DA, He W, Low PS, Wei A, Cheng JX (2005) In vitro and in vivo two-photon luminescence imaging of single gold nanorods. Proc Natl Acad Sci U S A 102(44):15752–15756
182. Loumaigne M, Richard A, Laverdant J, Nutarelli D, Débarre A (2010) Ligand-induced anisotropy of the two-photon luminescence of spherical gold particles in solution unraveled at the single particle level. Nano Lett 10(8):2817–2824
183. Durr NJ, Larson T, Smith DK, Korgel BA, Sokolov K, Ben-Yakar A (2007) Two-photon luminescence imaging of cancer cells using molecularly targeted gold nanorods. Nano Lett 7(4):941–945
184. Huff TB, Hansen MN, Zhao Y, Cheng J-X, Wei A (2007) Controlling the cellular uptake of gold nanorods. Langmuir 23(4):1596–1599
185. He W, Wang H, Hartmann LC, Cheng JX, Low PS (2007) In vivo quantitation of rare circulating tumor cells by multiphoton intravital flow cytometry. Proc Natl Acad Sci U S A 104(28):11760–11765
186. Liang G, Tegy JV, Vengadesan N (2011) Nanoshells for in vivo imaging using two-photon excitation microscopy. Nanotechnology 22(36):365102

187. Tong L, Cobley CM, Chen J, Xia Y, Cheng J-X (2010) Bright three-photon luminescence from gold/silver alloyed nanostructures for bioimaging with negligible photothermal toxicity. Angew Chem Int Ed 49(20):3485–3488
188. Wang LV (2008) Tutorial on photoacoustic microscopy and computed tomography. IEEE J Sel Top Quantum Electron 14(1):171–179
189. Wang Y, Xie X, Wang X, Ku G, Gill KL, O'Neal DP, Stoica G, Wang LV (2004) Photoacoustic tomography of a nanoshell contrast agent in the in vivo rat brain. Nano Lett 4(9):1689–1692
190. Jokerst JV, Cole AJ, Van de Sompel D, Gambhir SS (2012) Gold nanorods for ovarian cancer detection with photoacoustic imaging and resection guidance via Raman imaging in living mice. ACS Nano 6(11):10366–10377
191. Chen Y-S, Frey W, Kim S, Kruizinga P, Homan K, Emelianov S (2011) Silica-coated gold nanorods as photoacoustic signal nanoamplifiers. Nano Lett 11(2):348–354
192. Jokerst JV, Thangaraj M, Kempen PJ, Sinclair R, Gambhir SS (2012) Photoacoustic imaging of mesenchymal stem cells in living mice via silica-coated gold nanorods. ACS Nano 6(7):5920–5930
193. Li W, Brown PK, Wang LV, Xia Y (2011) Gold nanocages as contrast agents for photoacoustic imaging. Contrast Media Mol Imaging 6(5):370–377
194. Yang X, Skrabalak SE, Li Z-Y, Xia Y, Wang LV (2007) Photoacoustic tomography of a rat cerebral cortex in vivo with au nanocages as an optical contrast agent. Nano Lett 7(12):3798–3802
195. Song KH, Kim C, Cobley CM, Xia Y, Wang LV (2008) Near-infrared gold nanocages as a new class of tracers for photoacoustic sentinel lymph node mapping on a rat model. Nano Lett 9(1):183–188
196. Kim C, Cho EC, Chen J, Song KH, Au L, Favazza C, Zhang Q, Cobley CM, Gao F, Xia Y, Wang LV (2010) In vivo molecular photoacoustic tomography of melanomas targeted by bioconjugated gold nanocages. ACS Nano 4(8):4559–4564
197. Kim C, Song H-M, Cai X, Yao J, Wei A, Wang LV (2011) In vivo photoacoustic mapping of lymphatic systems with plasmon-resonant nanostars. J Mater Chem 21(9):2841–2844
198. Nie L, Wang S, Wang X, Rong P, Ma Y, Liu G, Huang P, Lu G, Chen X (2014) In vivo volumetric photoacoustic molecular angiography and therapeutic monitoring with targeted plasmonic nanostars. Small 10(8):1585–1593
199. Cheng K, Kothapalli S-R, Liu H, Koh AL, Jokerst JV, Jiang H, Yang M, Li J, Levi J, Wu JC, Gambhir SS, Cheng Z (2014) Construction and validation of nano gold tripods for molecular imaging of living subjects. J Am Chem Soc 136(9):3560–3571
200. Galper MW, Saung MT, Fuster V, Roessl E, Thran A, Proksa R, Fayad ZA, Cormode DP (2012) Effect of computed tomography scanning parameters on gold nanoparticle and iodine contrast. Invest Radiol 47(8):475–481
201. Hainfeld JF, Slatkin DN, Focella TM, Smilowitz HM (2006) Gold nanoparticles: a new x-ray contrast agent. Br J Radiol 79(939):248–253
202. Kim D, Park S, Lee JH, Jeong YY, Jon S (2007) Antibiofouling polymer-coated gold nanoparticles as a contrast agent for in vivo x-ray computed tomography imaging. J Am Chem Soc 129(24):7661–7665
203. Boote E, Fent G, Kattumuri V, Casteel S, Katti K, Chanda N, Kannan R, Katti K, Churchill R (2010) Gold nanoparticle contrast in a phantom and juvenile swine: models for molecular imaging of human organs using x-ray computed tomography. Acad Radiol 17(4):410–417
204. Kattumuri V, Katti K, Bhaskaran S, Boote EJ, Casteel SW, Fent GM, Robertson DJ, Chandrasekhar M, Kannan R, Katti KV (2007) Gum Arabic as a phytochemical construct for the stabilization of gold nanoparticles: in vivo pharmacokinetics and x-ray-contrast-imaging studies. Small 3(2):333–341
205. Peng C, Zheng L, Chen Q, Shen M, Guo R, Wang H, Cao X, Zhang G, Shi X (2012) PEGylated dendrimer-entrapped gold nanoparticles for in vivo blood pool and tumor imaging by computed tomography. Biomaterials 33(4):1107–1119

206. Chie K, Yasuhito U, Mikako O, Atsushi H, Yasuhiro M, Kenji K (2010) X-ray computed tomography contrast agents prepared by seeded growth of gold nanoparticles in PEGylated dendrimer. Nanotechnology 21(24):245104
207. Reuveni T, Motiei M, Romman Z, Popovtzer A, Popovtzer R (2011) Targeted gold nanoparticles enable molecular CT imaging of cancer: an in vivo study. Int J Nanomedicine 6:2859–2864
208. Sun I-C, Eun D-K, Koo H, Ko C-Y, Kim H-S, Yi DK, Choi K, Kwon IC, Kim K, Ahn C-H (2011) Tumor-targeting gold particles for dual computed tomography/optical cancer imaging. Angew Chem Int Ed 50(40):9348–9351
209. Eck W, Nicholson AI, Zentgraf H, Semmler W, Bartling S (2010) Anti-CD4-targeted gold nanoparticles induce specific contrast enhancement of peripheral lymph nodes in x-ray computed tomography of live mice. Nano Lett 10(7):2318–2322
210. Campion A, Kambhampati P (1998) Surface-enhanced Raman scattering. Chem Soc Rev 27(4):241–250
211. Moskovits M (2005) Surface-enhanced Raman spectroscopy: a brief retrospective. J Raman Spectrosc 36(6–7):485–496
212. Alvarez-Puebla RA, Liz-Marzan LM (2012) Traps and cages for universal SERS detection. Chem Soc Rev 41(1):43–51
213. Vo-Dinh T, Wang HN, Scaffidi J (2010) Plasmonic nanoprobes for SERS biosensing and bioimaging. J Biophotonics 3(1–2):89–102
214. Wachsmann-Hogiu S, Weeks T, Huser T (2009) Chemical analysis in vivo and in vitro by Raman spectroscopy-from single cells to humans. Curr Opin Biotechnol 20(1):63–73
215. Levin CS, Kundu J, Barhoumi A, Halas NJ (2009) Nanoshell-based substrates for surface enhanced spectroscopic detection of biomolecules. Analyst 134(9):1745–1750
216. Larmour IA, Graham D (2011) Surface enhanced optical spectroscopies for bioanalysis. Analyst 136(19):3831–3853
217. Qian X, Peng XH, Ansari DO, Yin-Goen Q, Chen GZ, Shin DM, Yang L, Young AN, Wang MD, Nie S (2008) In vivo tumor targeting and spectroscopic detection with surface-enhanced Raman nanoparticle tags. Nat Biotechnol 26(1):83–90
218. Park J-H, von Maltzahn G, Ong LL, Centrone A, Hatton TA, Ruoslahti E, Bhatia SN, Sailor MJ (2010) Cooperative nanoparticles for tumor detection and photothermally triggered drug delivery. Adv Mater 22(8):880–885
219. Samanta A, Maiti KK, Soh K-S, Liao X, Vendrell M, Dinish US, Yun S-W, Bhuvaneswari R, Kim H, Rautela S, Chung J, Olivo M, Chang Y-T (2011) Ultrasensitive near-infrared Raman reporters for SERS-based in vivo cancer detection. Angew Chem Int Ed 50(27):6089–6092
220. Kircher MF, de la Zerda A, Jokerst JV, Zavaleta CL, Kempen PJ, Mittra E, Pitter K, Huang RM, Campos C, Habte F, Sinclair R, Brennan CW, Mellinghoff IK, Holland EC, Gambhir SS (2012) A brain tumor molecular imaging strategy using a new triple-modality MRI-photoacoustic-Raman nanoparticle. Nat Med 18(5):829–835
221. Karabeber H, Huang R, Iacono P, Samii JM, Pitter K, Holland EC, Kircher MF (2014) Guiding brain tumor resection using surface-enhanced Raman scattering nanoparticles and a hand-held Raman scanner. ACS Nano 8(10):9755–9766
222. Keren S, Zavaleta C, Cheng Z, de la Zerda A, Gheysens O, Gambhir SS (2008) Noninvasive molecular imaging of small living subjects using Raman spectroscopy. Proc Natl Acad Sci U S A 105(15):5844–5849
223. Zavaleta CL, Smith BR, Walton I, Doering W, Davis G, Shojaei B, Natan MJ, Gambhir SS (2009) Multiplexed imaging of surface enhanced Raman scattering nanotags in living mice using noninvasive Raman spectroscopy. Proc Natl Acad Sci U S A 106(32):13511–13516
224. von Maltzahn G, Centrone A, Park JH, Ramanathan R, Sailor MJ, Hatton TA, Bhatia SN (2009) SERS-coded gold nanorods as a multifunctional platform for densely multiplexed near-infrared imaging and photothermal heating. Adv Mater 21(31):3175–3180

225. Maiti KK, Dinish US, Samanta A, Vendrell M, Soh KS, Park SJ, Olivo M, Chang YT (2012) Multiplex targeted in vivo cancer detection using sensitive near-infrared SERS nanotags. Nano Today 7(2):85–93
226. Kang H, Jeong S, Park Y, Yim J, Jun BH, Kyeong S, Yang JK, Kim G, Hong S, Lee LP, Kim JH, Lee HY, Jeong DH, Lee YS (2013) Near-infrared SERS nanoprobes with plasmonic Au/Ag hollow-shell assemblies for in vivo multiplex detection. Adv Funct Mater 23(30):3719–3727
227. Iacono P, Karabeber H, Kircher MF (2014) A "Schizophotonic" all-in-one nanoparticle coating for multiplexed SE(R)RS biomedical imaging. Angew Chem Int Ed 126(44):11950–11955
228. Kim J, Park S, Lee JE, Jin SM, Lee JH, Lee IS, Yang I, Kim JS, Kim SK, Cho MH, Hyeon T (2006) Designed fabrication of multifunctional magnetic gold nanoshells and their application to magnetic resonance imaging and photothermal therapy. Angew Chem Int Ed 45(46):7754–7758
229. Ji X, Shao R, Elliott AM, Stafford RJ, Esparza-Coss E, Bankson JA, Liang G, Luo Z-P, Park K, Markert JT, Li C (2007) Bifunctional gold nanoshells with a superparamagnetic iron oxide–silica core suitable for both MR imaging and photothermal therapy. J Phys Chem C 111(17):6245–6251
230. Chen W, Bardhan R, Bartels M, Perez-Torres C, Pautler RG, Halas NJ, Joshi A (2010) A molecularly targeted theranostic probe for ovarian cancer. Mol Cancer Ther 9(4):1028–1038
231. Bardhan R, Chen WX, Perez-Torres C, Bartels M, Huschka RM, Zhao LL, Morosan E, Pautler RG, Joshi A, Halas NJ (2009) Nanoshells with targeted simultaneous enhancement of magnetic and optical imaging and photothermal therapeutic response. Adv Funct Mater 19(24):3901–3909
232. Li Z, Yin S, Cheng L, Yang K, Li Y, Liu Z (2014) Magnetic targeting enhanced theranostic strategy based on multimodal imaging for selective ablation of cancer. Adv Funct Mater 24(16):2312–2321
233. Cheng L, Yang K, Li Y, Chen J, Wang C, Shao M, Lee ST, Liu Z (2011) Facile preparation of multifunctional upconversion nanoprobes for multimodal imaging and dual-targeted photothermal therapy. Angew Chem Int Ed Engl 50(32):7385–7390
234. Coughlin AJ, Ananta JS, Deng N, Larina IV, Decuzzi P, West JL (2014) Gadolinium-conjugated gold nanoshells for multimodal diagnostic imaging and photothermal cancer therapy. Small 10(3):556–565
235. Zhang Y, Qian J, Wang D, Wang Y, He S (2013) Multifunctional gold nanorods with ultrahigh stability and tunability for in vivo fluorescence imaging, SERS detection, and photodynamic therapy. Angew Chem Int Ed Engl 52(4):1148–1151